DEVELOPMENT OF RESPONSE SURFACE DATA ON THE HEAD INJURY CRITERIA ASSOCIATED WITH VARIOUS AIRCRAFT AND AUTOMOTIVE HEAD IMPACT SCENARIOS

A Thesis by

PrasannaVadanan Nallan Chakravarthy

Bachelor of Engineering, Osmania University, 2013

Submitted to the Department of Mechanical Engineering
and the faculty of the Graduate School of
Wichita State University
in partial fulfillment of
the requirements for the degree of
Master of Science

July 2016

DEVELOPMENT OF RESPONSE SURFACE DATA ON THE HEAD INJURY CRITERIA ASSOCIATED WITH VARIOUS AIRCRAFT AND AUTOMOTIVE HEAD IMPACT SCENARIOS

The following faculty members have examined the final copy of this thesis for form and content, and recommend that it be accepted in partial fulfillment of the requirement for the degree of Master of Science with a major in Mechanical Engineering.

_____
Hamid Lankarani, Committee Chair

_____
Krishna Krishnan, Committee Member

_____
Rajeev Madhavannair, Committee Member

DEDICATION

To my parents, friends and family

and

To my advisor, Dr. Hamid Lankarani

ACKNOWLEDGEMENTS

I am really thankful to my advisor, Dr. Hamid Lankarani, Professor of Mechanical Engineering Department at Wichita State University, for all his guidance and support throughout my studies. His encouragement and patience helped me complete this thesis.

I would like to thank my committee members Dr. Rajeev Madhavannair and Dr. Krishna Krishnan for their valuable time in reviewing this thesis.

I would also like to thank my friends Subhadra Gudimella, Sneha Reddy, Pranay Kumar, Sumanth Kumar, Kushal Reddy, Sudhamsh Bijjala, Wilson Pramod, Bhargav Sai, Yeshwanth Reddy, Vishal Krishna, Suresh Venkata, Nitheesh Sasikumar, Mohammad Salahuddin, Mohammad Arfath, Tajamul Hussain, Viquar Hassan, Bhuvija Odapally, Pankaj Salunke, Aneesha Gogineni, Ranjeeth Kumar, Rohit Kolluru, Saketh Reddy, and Vijay Sai for their constant support and making my stay in Wichita pleasant.

Finally, I would take this opportunity to thank my parents Mrs Bama & Mr. Balajee, my sister Pavitra, my brother-in-law Mohit and my little niece Anyusha for their love, support and constant encouragement throughout my master's studies.

ABSTRACT

Safety of passengers in both automotive and aircraft is always looked upon for more advancement in providing better safety and minimizing the injuryies/fatalities during crashes. Among the injuries which are incurred onto the occupants in both aviation and automotive accidents, the head injuries are the most fatal and severe type of injury. In aircraft accidents, mostly in the event of air turbulence or emergency landing, the passengers seated behind bulkheads or interior walls have a higher chance of head impact onto these structures. Similarly, the vehicle safety is considered to be quiet important for automobile manufacturers as well as customers. Among all automobile crashes, frontal impact collisions are the most common types of crash scenario. The most observed injuries in these crashes is caused by the impact of the head to the steering wheel, windshield, etc. This thesis presents an investigation and development of response surface data on the Head Injury Criteria (HIC) during frontal crashes in both automotive and aircraft accidents. Consideration is made relative to the Federal Aviation Regulations (FARs) for the aircraft industry and the US-NCAP (New Car Assessment Program) protocol for frontal impact crashes in automotive industry. For this purpose, a hybrid III 50^{th} percentile dummy is utilized in the occupant modeling code MADYMO to investigate the variations of the HIC with different parameters such as impact speed, impact angle, seat belt properties, seat pitch distances, and stiffness or material properties of the impact surface. Finally, a Design-of-Experiments (DOE)/Kriging model is utilized to generate response surface data on the HIC, using the sample results obtained from the MADYMO computer models. The collective results of the many simulations as surface plots from this study could be of significant use to the designers of automotive seats and aircraft interiors and in coming up with the most promising designs for occupant head impact protection in various frontal crash scenarios.

TABLE OF CONTENTS

Chapter **Page**

TABLE OF CONTENTS (continued)

Chapter **Page**

LIST OF TABLES

Table **Page**

LIST OF FIGURES

Figure **Page**

LIST OF FIGURES (continued)

Figure **Page**

LIST OF FIGURES (continued)

Figure **Page**

LIST OF FIGURES (continued)

Figure **Page**

ABBREVIATIONS LIST

Symbols	Description
FAA	Federal Aviation Administration
FAR	Federal Aviation Regulation
NCAP	New Car Assesment Program
HIC	Head Injury Critreria
MADYMO	Mathematical Dynamic Model
DOE	Design of Experiment
FE	Finite Element
FEM	Finite Element Method
FEA	Finite Elemnt Analysis

CHAPTER 1

INTRODUCTION

1.1 Background

Among all the injuries, the head injury is considered to be most common and severe injury of all accidents. The injuries to the head can occur at low and high speeds, and even if the head does not impact on a solid object. Even with all safety features and technology available, statistics show head remains vulnerable to accidents. The probability of head injuries increases even more when a driver or passenger fails to wear a seat belt. Figure 1.1 shows to the percentage of head injury and its causes, with motor vehicle and traffic related records highest percentage of head injuries.

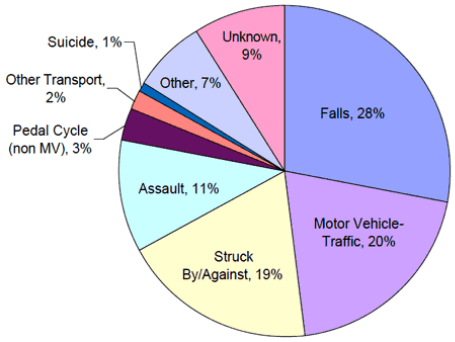

Figure 1.1: Percentage of brain or head injury death [1]

In an aviation related accidents, the year 2015 was turned to be a quite safe year for commercial aviation, with aviation safety network recording 521 fatalities [2]. As per the aviation safety network, the stats collected reports suggest that the accident related to aviation is a record low for last 60 years, if the suicides and sabotage is neglected. Figure 1.2 illustrates to the aviation related accident and fatalities data over the years, with 2015 having the least number of accidents over the last 50 years, and Figure 1.3 shows the number of accidents by aviation type in the year 2015, with General aviation recorded the highest number of accidents.

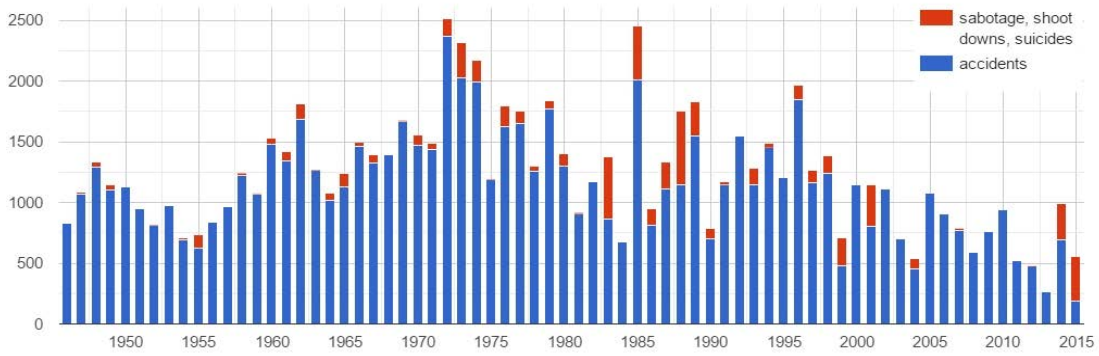

Figure 1.2: shows the fatalities and accident data over the years [2]

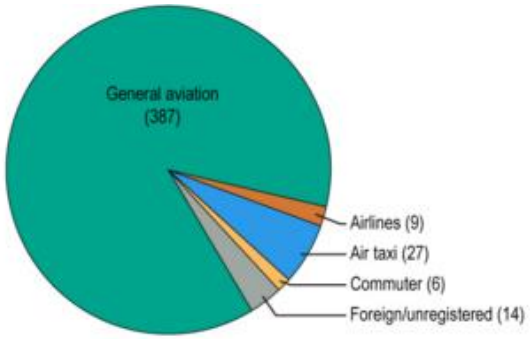

Figure 1.3: Number of accidents by aviation types [2]

Head injuries in the aircraft could be due to impacting the head on to the any of the following surface:

- Bulkhead
- Windscreen
- Front seats
- Cabin side wall

The sudden change of acceleration during the crash causes the head to impact on the bulkhead. Bulkheads are the partition or a dividing wall in an airplane, and also provide structural support for the aircraft. Figure 1.4 shows an experimental setup of dummy impacting the bulkhead.

Figure 1.4: Experimental setup of dummy impacting on bulkhead [18]

Bulkheads are the partition or a dividing wall in an airplane, and also provide structural support for the aircraft. The seats behind the dividing wall are called as bulkhead seat, which means there is no seats in front of you and there is more legroom space available. Although, some people prefer for bulkhead seats because of the space available, but, during a crash scenario large force up to 16 G's is experienced by passengers seated in the aircraft and vulnerable to head impact on to the bulkhead which could result in very serious injury. At the same time it is tough for the aviation industry to remove the bulkhead seats, as it could result in huge net revenue loss.

Similarly, the automobile accident can be a terrifying experience with the people involved are injured severely and virtually injuring any part of the body depending on the severity and circumstance of the crash. According to National Highway Traffic Safety Administration (NHTSA) latest report, there is a steep inclination of traffic related death, which shows there is a 9.3 % increase only for the first nine months of 2015 [3]. It further added that the estimation of death in first 9 month was 26,000 when compared to 23,796 in 2014, registering the highest increase in year to year from last 50 years. Figure 1.5 shows the fatality rate over the year for the automobile accidents.

Table 1.1: Fatality rate over the year for the automobile accident [3]

Quarter	1st Quarter (Jan–Mar)	2nd Quarter (Apr–Jun)	3rd Quarter (Jul–Sep)	4th Quarter (Oct–Dec)	Total (Full Year)	1st Nine Months (Jan–Sep)
Fatalities and Percentage Change in Fatalities for the Corresponding Quarter/Half From the Prior Year						
2005	9,239	11,005	11,897	11,369	43,510	32,141
2006	9,558 [+3.5%]	10,942 [-0.6%]	11,395 [-4.2%]	10,813 [-4.9%]	42,708 [-1.8%]	31,895 [-0.8%]
2007	9,354 [-2.1%]	10,611 [-3.0%]	11,056 [-3.0%]	10,238 [-5.3%]	41,259 [-3.4%]	31,021 [-2.7%]
2008	8,459 [-9.6%]	9,435 [-11.1%]	9,947 [-10.0%]	9,582 [-6.4%]	37,423 [-9.3%]	27,841 [-10.3%]
2009	7,552 [-10.7%]	8,975 [-4.9%]	9,104 [-8.5%]	8,252 [-13.9%]	33,883 [-9.5%]	25,631 [-7.9%]
2010	6,755 [-10.6%]	8,522 [-5.0%]	9,226 [+1.3%]	8,496 [+3.0%]	32,999 [-2.6%]	24,503 [-4.4%]
2011	6,726 [-0.4%]	8,227 [-3.5%]	8,984 [-2.6%]	8,542 [+0.5%]	32,479 [-1.6%]	23,937 [-2.3%]
2012	7,521 [+11.8%]	8,612 [+4.7%]	9,171 [+2.1%]	8,478 [-0.7%]	33,782 [+4.0%]	25,304 [+5.7%]
2013	7,166 [-4.7%]	8,207 [-4.7%]	9,025 [-1.6%]	8,496 [+0.2%]	32,894 [-2.6%]	24,398 [-3.6%]
2014	6,843 [-4.5%]	8,171 [-0.4%]	8,782 [-2.7%]	8,879 [+4.5%]	32,675 [-0.7%]	23,796 [-2.5%]
2015[a]	*7,375 [+7.8%]*	*8,850 [+8.3%]*	*9,775 [+11.3%]*	—	—	*26,000 [+9.3%]*
Fatality Rate per 100 Million Vehicle Miles Traveled (VMT)						
2005	1.32	1.42	1.54	1.54	1.46	1.43
2006	1.35	1.41	1.47	1.44	1.42	1.41
2007	1.31	1.35	1.41	1.37	1.36	1.36
2008	1.22	1.25	1.33	1.32	1.26	1.26
2009	1.09	1.16	1.17	1.12	1.15	1.14
2010	0.98	1.09	1.18	1.14	1.11	1.09
2011	0.98	1.09	1.18	1.17	1.10	1.09
2012	1.08	1.12	1.21	1.16	1.14	1.14
2013	1.04	1.07	1.17	1.15	1.10	1.09
2014	0.99	1.03	1.11	1.16	1.07	1.05
2015[a]	*1.03*	*1.08*	*1.19*	—	—	*1.10*

This, in fact, increased the medical expenses, productivity loss and property loss, increased 24% to roughly $ 152 billion [3]. Although the no of death percentage have been declined from 2000 to 2014, but the sudden inclination of death from 2014 to 2015 gives us signals that we need to do more. Figure 1.5 shows the death or the fatality percentage by type of road user, with car occupant recorded for highest percentage.

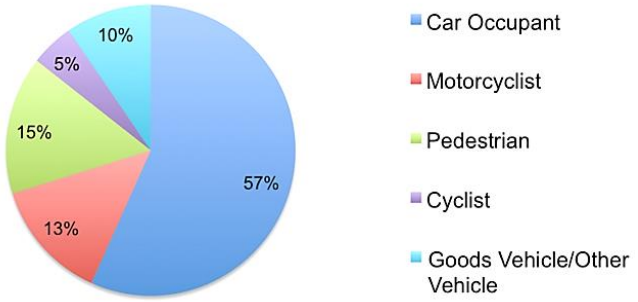

Figure 1.5: Death or fatality percentage for type of road user [3]

In automotive accidents, one of the common injuries suffered by the passenger is head and face injuries. The amount of force generated in an automobile accident can drive the person's head on to the windshield, side window and vehicle frame causing a serious injury, if the head is impacted on any one of them. Even though the head is being protected from the

impact on to the foreign objects with many safety features with no physical sign of trauma, there is still a considerable high risk of brain being jolted inside the skull because of the impact of a crash which could result is concussion and other injuries.

1.2 Crashworthiness

Crashworthiness is a term defined to describe the ability of a structure of an automobile or aviation to protect the occupant on an event of a crash or accident. During a collision the occupant is subjected to a large force which could result in serious injury, so the structure of an aircraft or automobile should be designed in such a way that the structure takes all the forces or help to reduce the force that are transmitted to the occupant. Many research is being conducted by many organizations and agency in providing better safety for occupants, where the research work mostly based on analytical and computation model which helps to predict the response of the fuselage structure and occupant in the event of a crash. In automotive, the National Highway Traffic Safety Administration is responsible for developing test procedure and evaluating motor safety.

1.3 Head Injury Criteria (HIC)

In this study, to examine the injury caused to the occupant's head due to the impact onto the bulkheads and impact surface Head Injury Criteria is used. US government, in response to study by “Versace", developed a new injury criterion for the head called the Head Injury Criterion [29].

$$HIC = max\left[\frac{1}{t_2-t_1}\int_{t_1}^{t_2} a(t)dt\right]^{2.5}(t_2 - t_1) \quad (1.1)$$

Where: a (t) is the resultant head acceleration in G’s (measured at the head’s center of gravity)

t_1 and t_2 are the initial and final times (in sec) during which HIC attains a maximum value.

HIC has a concussion tolerance level for the frontal collision or impact, i.e. should not exceed more than 1000. Time interval greatly affects the HIC calculation, the maximum time interval was set to 36 ms by the automotive industry. Over the years the time interval has decreased gradually to avoid the use of HIC to hard contact/ impacts and the limit also has been reduced to 700. The HIC value has been shown to be quite sensitive and depends on many parameters such as the impact angle, impact velocity and impact surface stiffness etc.

1.4 Aircraft Seat Certification Standards

Federal Aviation Regulation sets of rules and regulation which was established by the Federal Aviation Administration (FAA), which is governing the aviation guidelines in America, it is also responsible for production approval, certifications of safety related issues [14]. Some of its specific test requirements are:

- FAR Part 23 (pilot and passenger) for General Aviation Aircraft
- FAR Part 25 for Transportation aircraft
- FAR Part 27 for Rotorcraft

To study the responses of human body these two test conditions have been proposed. The test procedures are carried out for vertical impacts on the ground and the forward direction crash scenario, as shown in the Figures 1.6 and 1.7. In the first test condition, the dummy seat setup is inclined at an angle of 60 degrees with the horizontal and G-force and velocity change are calculated. The obtained results are comparatively lower and in the second test condition, the dummy and seat set up are placed in a forward direction impact test, and the results obtained are relatively higher than the test condition 1. The main purpose of these two tests was to study the

nature of restraining system, occupant safety, seating system and deformation during the crash or emergency landing.

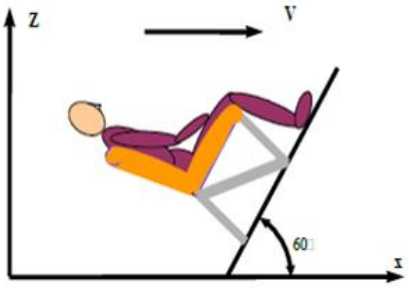

Figure 1.6: Test-1 condition **[**22**]**

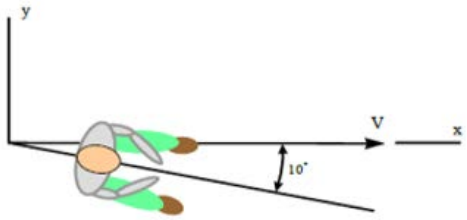

Figure 1.7**:** Test -2 condition [22]

Figure 1.7 and 1.8 shows the graphical representation of test 1 and test 2 condition according to the FAA

1.4.1 Federal Aviation Regulation Part 23

Figure 1.9 illustrates the acceleration pulses versus time for Part 23 passenger and pilot for the regulation test 2 condition. The acceleration peak values are different for pilot and passenger. For the passenger, the acceleration exposed is set to 21 G's, and for the pilot, it is up to 26 G's which is slightly higher than for a passenger.

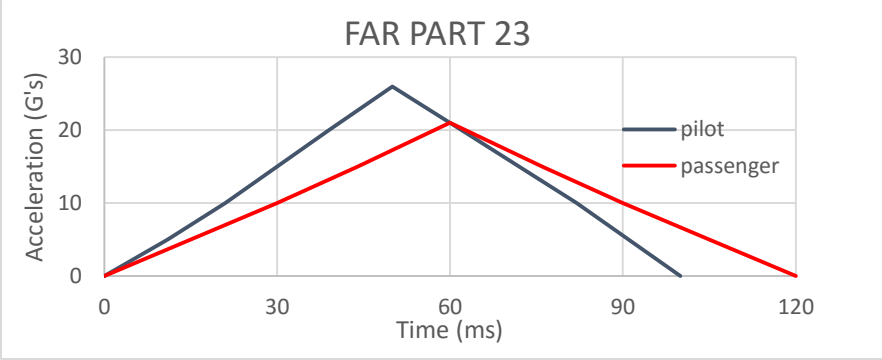

Figure 1.8: Acceleration vs time for passenger and pilot in FAR Part 23 Test-2 condition

1.4.2 Federal Aviation Regulation Part 25

Figure 1.10 shows the acceleration versus time for Test 2 condition Part 25. The acceleration peak value during crash scenario is less when compared to Part 23 and the acceleration values is same for both pilot and passenger. The highest peak acceleration recorded during a crash scenario is 16 G's. Therefore the head injury and other injury would be far lesser than Part 23.

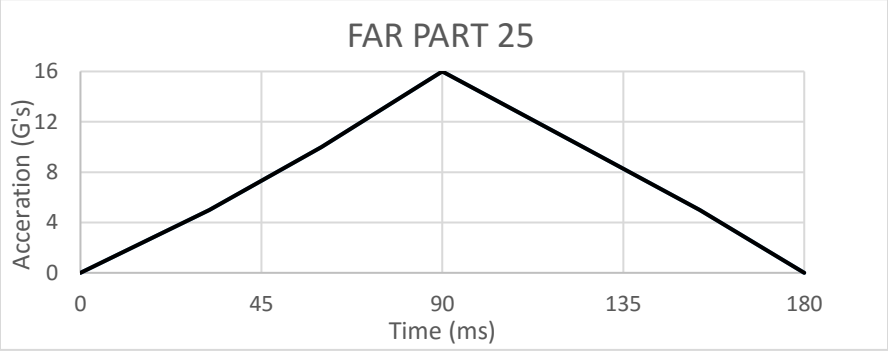

Figure 1.9: Acceleration vs time for FAR part 25 test 2 condition

Table 1.1: Federal Aviation Regulations test conditions 1 and 2

Test Condition 1	PART 23		PART 25	PART 27
	Pilot	Passenger		
Velocity change (ft/sec)	31	31	35	30
Acceleration Pulse (G's)	19	15	14	30
Rise Time (sec)	0.05	0.06	0.08	0.031
Test Condition 2	PART 23		PART 25	PART 27
	Pilot	Passenger		
Velocity Change (ft/Sec)	42	42	44	42
Acceleration Pulse (G's)	26	21	16	18.4
Rise Time (sec)	0.05	0.06	0.09	0.071

1.5 Full Frontal Rigid Barrier Impact Test

Full frontal barrier impact test represents a vehicle impacting on a rigid surface of a typical sedan, in this study a Ford Taurus car is used. This test is intended to represent the most common crash of the real world with impact direction perpendicular to the fixed barrier and the test was carried out for 35 mph speed. Figure 1.10 refers to the NCAC full frontal rigid barrier impact test setup [33]. The finite element modeling of the Ford Taurus car in this thesis has been developed at the National Crash Analysis Center.

Figure 1.10: NCAC Full frontal rigid barrier impact test

In this test, the vehicle velocity is changed when the impact on the rigid surface takes place because of the there is sudden deceleration. The dummy is placed in the front seats and the injuries pertaining to the dummy is studied. Among all the injury, head, neck and lower torso injuries were the critical injury which was observed. This test is very useful and studies about the injuries of occupant and restraining system. However, it does not study the structural integrity of the vehicle. This rigid barrier impact test is standard crashworthiness not only in U.S but also in Australia, Canada and Japan.

1.5.1 FMVSS Regulations

To improve the passenger Safety, National Highway Traffic Safety Administration has proposed certain regulation; among the regulation FMVSS 208 is to measure the occupant safety

in a serious frontal collision. This regulation was proposed in 1960 and was intended to minimize the road accident, injuries and death with respect to frontal collision, every automobile manufactured are supposed to show compliance with this regulation and mandate to meet the safety standards proposed under this regulation.

This regulation was primarily proposed to address the safety issue related to front seat passengers in the event of a crash or frontal collision. For this, at various test condition and procedure were proposed to examine the possible and serious injuries caused due to frontal impact. To address and evaluate the regulation and study the response of the occupant and vehicle structure during the crash few o test conditions was proposed, which were the most common frontal collision impact scenario recorded in the real world. Some of the test condition is [11]:

- Full frontal barrier test
- Oblique frontal fixed barrier test
- Offset frontal barrier test
- Generic sled test
- Moving Perpendicular deformable barrier
- Fixed deformable barrier test
- Moving oblique barrier test

1.6 Literature Review

Significant information for various Federal Aviation Regulations on aircraft seat, certification and information on the safety features from the regulation and in depth evaluation on FAR PART 23, 25 can be found in this website [4]. Federal Motor Vehicle Safety Standard

(FMVSS) No. 208 information to measure how well a passenger vehicle would protect its occupants in the event of a serious real world frontal can be found from the sources [5]. Contact force modelling for HIC, bulkhead to frontal structure can be evaluated using several sources [6, 7, 8]. The evaluation of HIC and algorithms for such can be found in [9, 10].

Lankarani [16], Developed a Head Injury Criteria (HIC) Tester for Aircraft Seat Certification to address the problem faced in the certification of 16 g with airline seats located behind the bulkhead or class divider. In this research an alternate testing method for the evaluation of HIC without consumption of seats were addressed and further presented about several component testers which was developed primarily to study like, Free motion Head form, Pendulum test rig tester, Bowling ball tester and MGA neck/head impactor. Several other sources deal with aircraft injury and HIC evaluation [13, 14, 15].

Prabhu [37], conducted experiments to study the head path and HIC for aircraft seats using the Federal Aviation Regulation (FAR) Part 25 and Part 23 and presented a parametric study to show how the HIC and the head path varies. The objective of this study was to find best possible stiffness of the bulkhead and a possible set of parameters which can be used to reduce the fatalities in an aircraft accident.

For the automotive, the details of several FE models of various car categories can be found from in NCAC [33]. And information regarding full frontal barrier impact test and objective of the FMVSS 208 regulation can. It further gives information about the various test condition and exclusively for frontal impact. It further gives information about the possible consequence of various test condition for various speed and impact angle for different cars.

[33], information regarding the finite element model of ford Taurus passenger sedan car and gives injuries pertaining to the detailed information about various crashes for frontal collision like full frontal rigid barrier, oblique and offset collision and structural deformation pertaining to the crashes for different speed. It further gives information regarding vehicle to a vehicle frontal collision and side impact collision, acceleration and velocity changes for the rear and cross seat members, acceleration of the bottom and top of the engine and the structural deformation. Several other sources also have similar data on automotive injuries and HIC related injuries [30,32].

The Kriging based model was also used in a study for the dynamic of mechanical systems with revolute joints [12]. In terms of design of experiment (DOE), some sources utilize the Kriging model to develop a response surface methodology for a set of output in relation to several input variable [11,12].

1.7 Motivation

This thesis is motivated by existing research on aircraft and automotive crashworthiness, where every year, many people are injured or lose their lives in Automotive and Aircraft frontal direction accidents, among all the injury, the head injury is the most common and severe injuries faced by the occupants. The Head Injury Criteria (HIC), which is used to examine the severity of head injury, are quite sensitive to many input parameters and impact conditions. It would be quite useful to develop a database of the HIC values and impact parameters observed during automotive interior and aircraft seat testing regulations. And this database could be used by designers in predicting of potential head injuries and methods to address them.

CHAPTER 2

OBJECTIVES AND APPROACH

2.1 Objectives

The head being the most important part of the body, with any severe injury caused to the occupant's head during the event of a crash could result in fatalities. The objective of this study is to develop a set of Head injury Criteria (HIC) data using a response surface methodology for the various aircraft and automotive impact scenarios. In particular, the aim is to investigate how the HIC is varied with impact angle, impact velocity, belt property, impact surface material and seat pitch. Finally, Response surfaces are created from the data on the HIC by using the Kringing method in MATLAB which would be a representation of 3D surface plot.

2.2 Methodology

To achieve the above objective, the majority of this research was conducted using the biodynamic occupant multibody and MADYMO. Finite Element tools like MADYMO, LS-PREPOST as well as MATLAB programing. For this study, the thesis is divided into two parts, namely, aircraft and automotive accidents. To study the impact scenario in aircraft condition, an occupant seat model was developed in MADYMO and input parameters are given using the FAR regulation to the MADYMO model and results are obtained for various seat pitch, belt properties and Stiffness of impact surface. Similarly, for the automotive condition, using the FMVSS regulations, a full-frontal impact test is simulated for a rigid barrier impact. The acceleration pulse measured at the driver seat is imported into the occupant seat model in MADYMO, and simulation results are obtained for the various belt properties, stiffness of impact surface and different distances from a dummy head to steering presentation. Using the results obtained for aircraft and automotive, input condition a response surface data are created

using a DOE-based Kriging model. The overall methodology is shown in Figures 2.1, 2.2 and 2.3 in the form of a flowchart for aircraft, automotive, and Kriging model.

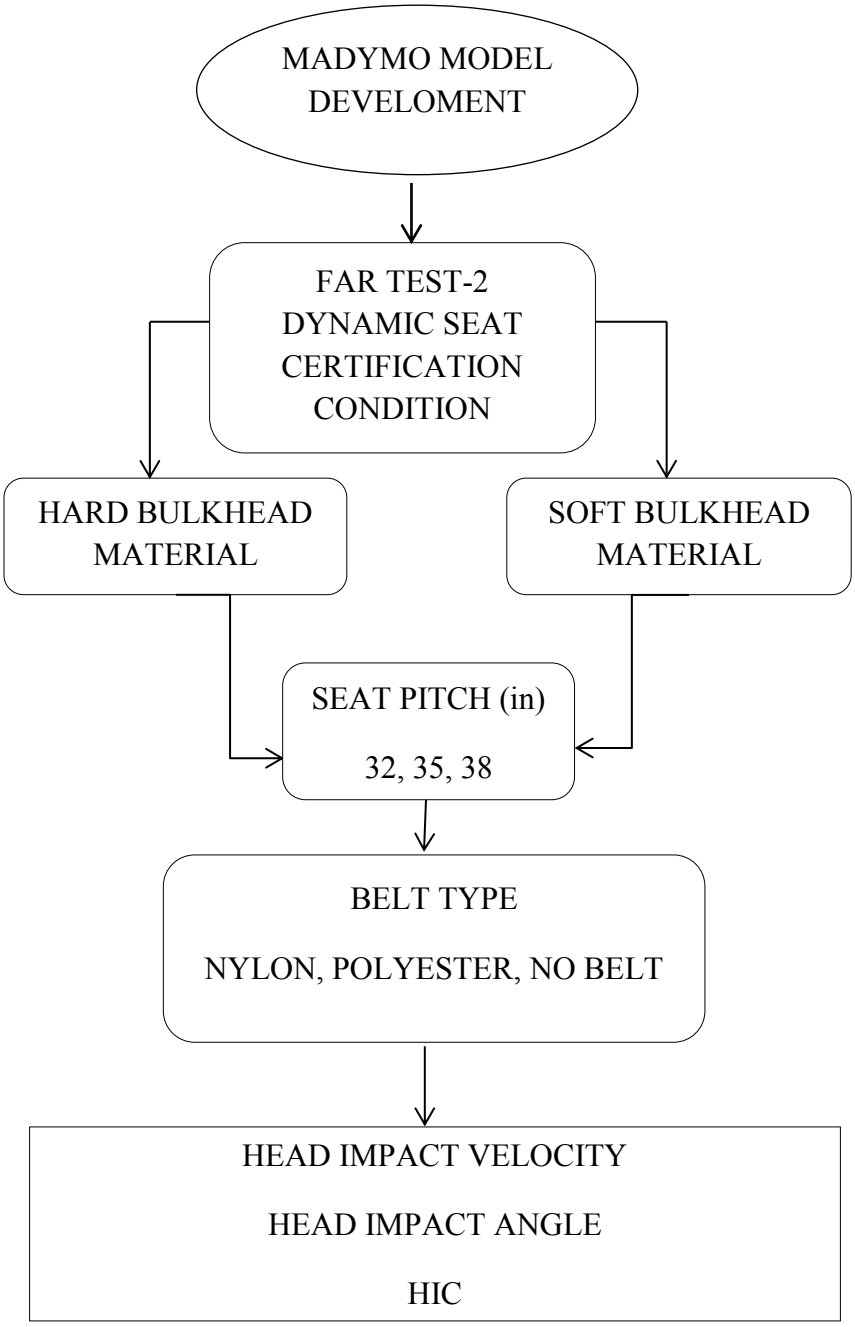

Figure 2.1: Flow chart representation of method of approach for aircraft frontal crashes investigation.

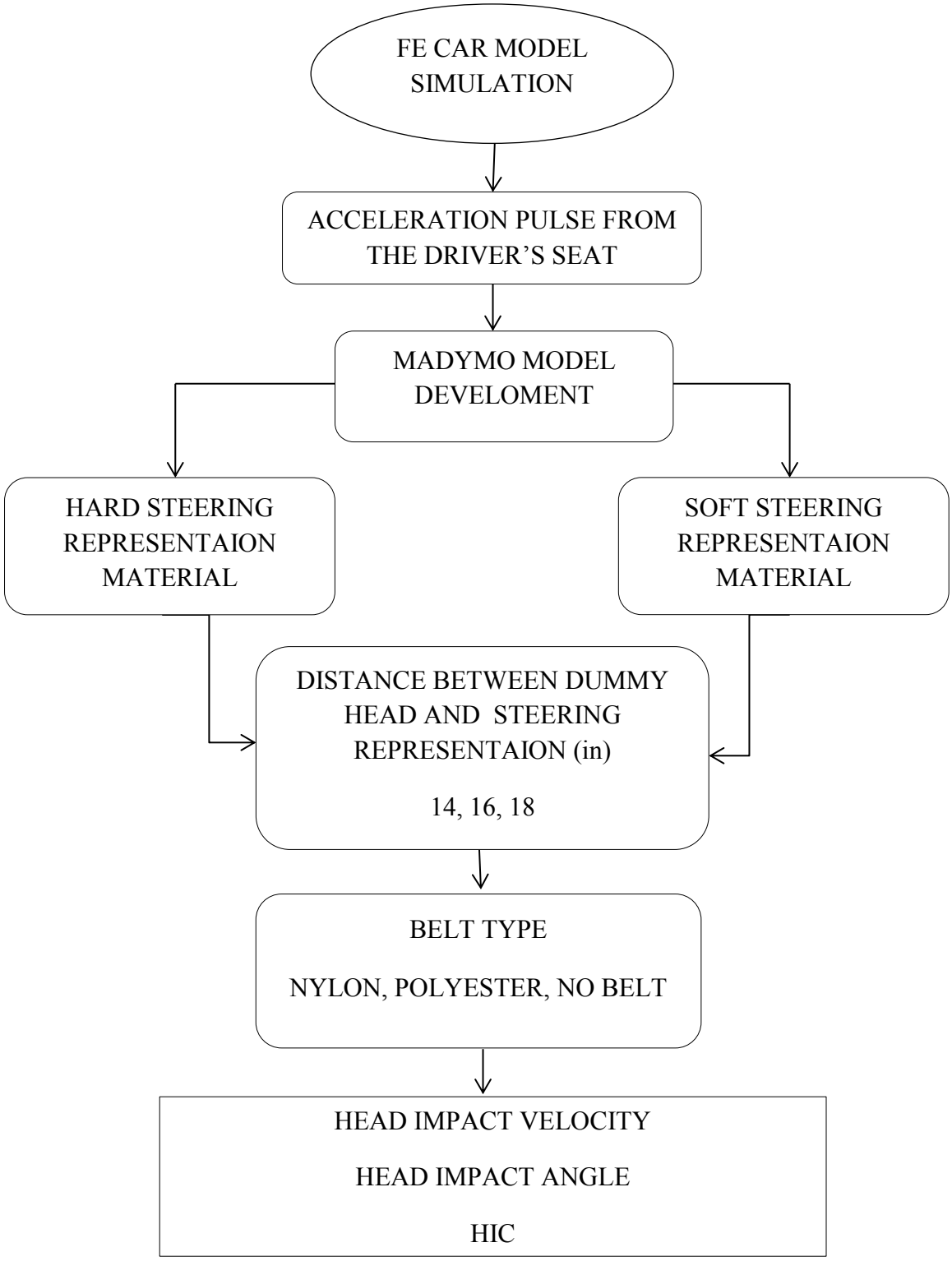

Figure 2.2: Flow chart representation of method of approach for automotive frontal crashes investigation.

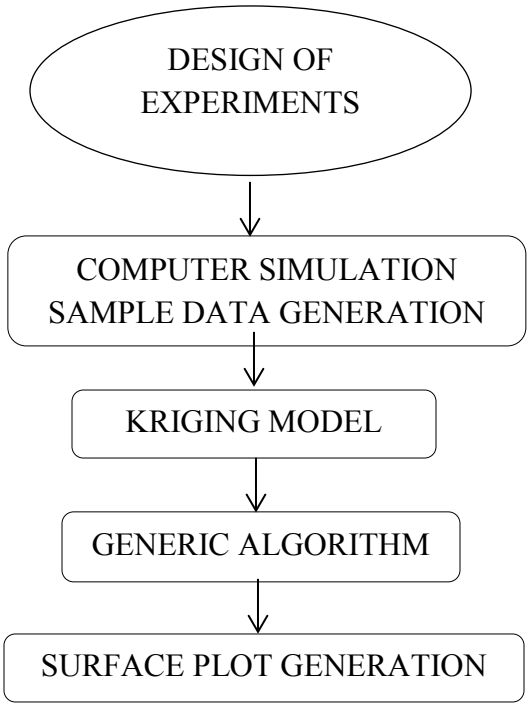

Figure 2.3: Flow chart representation of DOE and Kriging model.

2.3 Computational Tools

In recent years, for the support of analysis or design, computational tools are extensively utilized. These computational tools help in reducing the cost and time, as many of input variables can be varied each time, which makes research easy and efficient. Although, for the computational tools can never replace the physical test, validated models could be of significant can be of significant use in design evaluation and parametric studies. The following are the computational tool used in this thesis:

- LS-PREPOST
- MADYMO
- MATLAB

2.3.1 LS-DYNA

LS-DYNA is a finite element solver where mainly nonlinear, thermal and dynamic analysis problems are solved and the LS-PREPOST is used as pre and post processor for the LS-DYNA [40]. As a pre-processor, the LS-PREPOST can be used for various applications such as dummy positioning, belt fitting, airbag folding, penetrating checking, metal forming, scaling etc. After the solver finishes the siimulation of a particular mode, the result files are imported to LS-PREPOST for post-processing operations such as animation, graphical representation, stress distribution analysis etc. The other important property of LS-PREPOST is that it can input the result of various file format and export the data in different format.

2.3.2 MADYMO

Mathematic Dynamic Model (MADYMO) is used extensively in this thesis as a tool for multibody dynamic modeling and simulating of the aircraft and automotive occupant in various frontal impact scenarios [39]. It is useful for the reconstruction of crashes, study of safety feature like seat belts, airbags and is also considered to be very efficient and cost effective. This program is widely used by leading automotive, defense and aviation industries for correlating the experimental test data. The MADYMO solver supports both finite element model and multibody. In addition, a coupling function is also supported by MADYMO program with other finite element programs like radios, Pam-crash, ABAQUS and LS-DYNA for stimulation. A wide range of dummy models are used in this tool like Hybrid III dummies, side impact dummies, child dummies, pedestrian model and human model.

With respect to reference space, a coordinate system of X, Y, Z is connected and selected arbiraily to the origin and orientation of space coordinate system, where X is in the forward

direction and Z axis pointing upwards opposite to gravity, as shown in the Figure 2.4. The motion is described relative to this coordinate system.

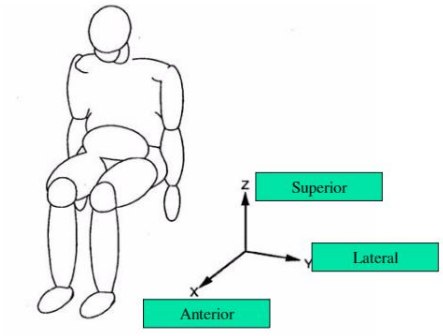

Figure 2.4: Reference space coordinate system [22]

A pair of bodies can be connected by a kinematic joint and a relative motion to this pair of body is said to be constrained with this kinematic joint. So, a relative translation is only allowed by translational joint. Because of these constrain on the kinematic joint there is load on 2 bodies, which restrict the relative motion for this pair of bodies and these constrain load are equal, but opposite loads and can be used to test the strength of the joint. The most common and different type of joints available in this tool are such as, revolute joint, spherical joint, cylindrical joint, translational joint, planar joints and universal joints.

2.3.3 MATLAB

MATLAB (matrix laboratory) is a programming language developed my Mathworks. It is used for plotting of function, data, use of algorithm, making a user interface for all the program and comparable to other programs like C, C++. Some of the key features of this MATLAB software are, it is a high level language for computing, and a customer user interface, graphic visualization tools, and application for data classification and control system.

CHAPTER 3

COMPUTATIONAL MODELING AND SIMULATIONS OF HEAD IMPACTS IN VARIOUS FRONTAL IMPACT SCENARIOS

3.1 Aircraft Occupant Head Impact Modeling

The overall aircraft occupant/belt/seat/bulkhead model representation is developed in MADYMO using planes, as shown in Figure 3.1. The upper seat where the back is resting is a plane of 23 inches height and inclined vertically with an angle of 14 degrees. The bulkhead plane is of 35 inch height and 40 inch width, placed at 32, 35 and 38 inches from the seat buckle for the separate set of simulation. Then, the Hybrid III dummy is imported and adjusted to an upright position. Finally, a two-point seatbelt model is developed and adjusted onto the dummy. In these simulations, two stiffness properties of bulkhead have been used, namely, hard (steel), and soft (Aluminum). The contact stiffness for the bulkhead or impact surface is calculated. Similarly, the belt properties are given using the loading and unloading characteristics. Two different belt types used for stimulations, namely nylon, and polyester.

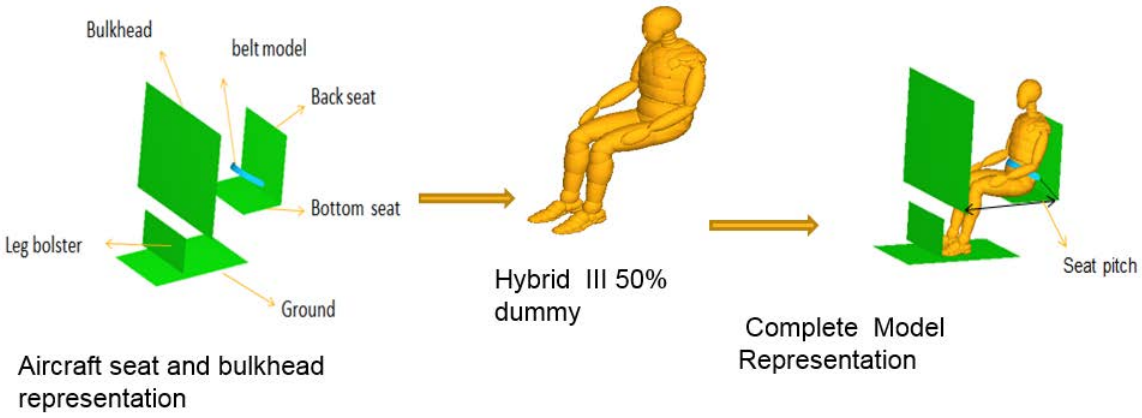

Figure 3.1: Aircraft occupant interior modeling representation in MADYMO.

3.2 Automotive Occupant Head Impact Modeling

3.2.1 FE Simulation of Vehicle Frontal Impact using LS-Dyna

The FE model of a typical sedan Ford Taurus vehicle and the rigid barrier model have been downloaded from NCAC website [36]. This FE model shown in the Figure 3.2, consists of 802 parts, 921793 nodes, 838880 shells, 10 beams, 134449 solids, 973351 elements and several accelerometer. The accelerometer is placed in this FE model, to compare the simulation result and with actual test results. Some of the locations where the accelerometer placed is: Engine bottom, engine top, right seat, left seat, seat cross member and lower B-pillar.

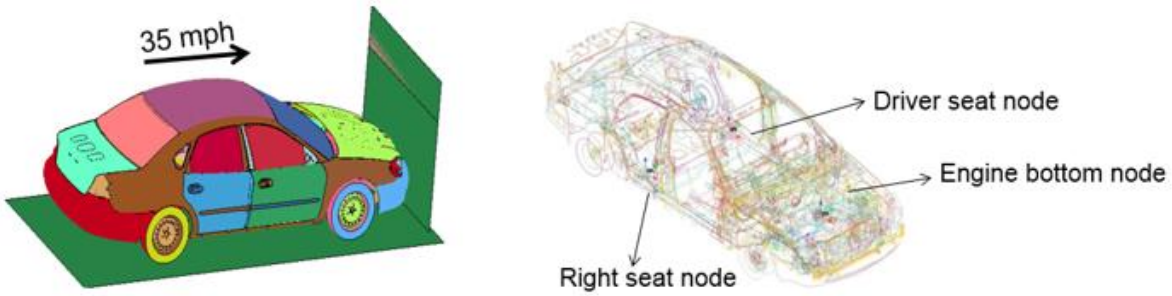

Figure 3.2: FE model of Ford Taurus [36]

The Ford Taurus frontal rigid barrier impact test is simulated using, the LS-DYNA/LS-PREPOST code. The FE car model is imported from the NCAC website and subjected to the frontal impact the rigid wall with a speed of 35 mph according to NCAP protocol. For 15-ms of FE car input simulation, a computational time required to run this model was ten hours. The Figure 3.3 shows the animation sequence and different stages of deformation of the car during simulation. Figure 3.4 shows the frontal shape of car post impact test of the car.

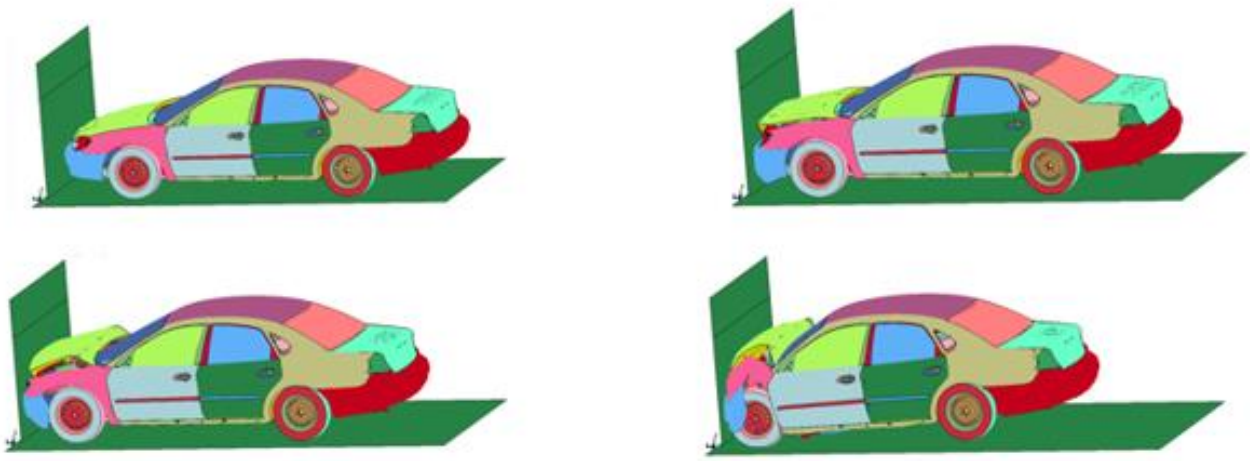

Figure 3.3: Animation sequence for frontal crash of the vehicle for US-NCAP

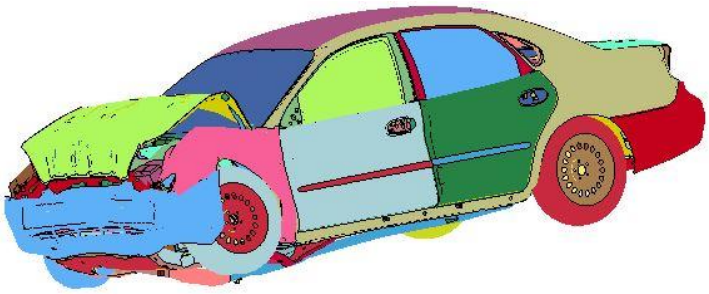

Figure 3.4: Ford Taurus post Frontal impact test.

3.2.2 Automotive FE Model Simulation Results and Validation

The crash simulation of ford Taurus is verified by comparing the results obtained with the actual frontal impact test. The NCAP Test 3248 is the frontal impact test performed in accordance with NCAP protocol. Figure 3.5 shows the acceleration of Engine top with the simulation and test result. The analysis graph is close enough to prove that the FE model of the vehicle is valid.

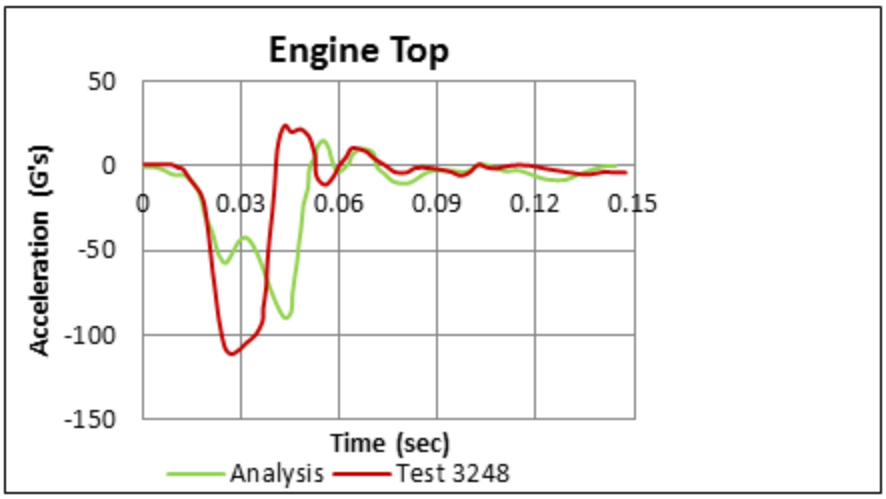

Figure 3.5: Validation graph Engine top Acceleration

Similarly, the graph of the average velocity of the seat cross member against time is compared to the simulation new test result. The results shown in the Figure 3.6 depicts similar behavior, thus validating the FE model with test.

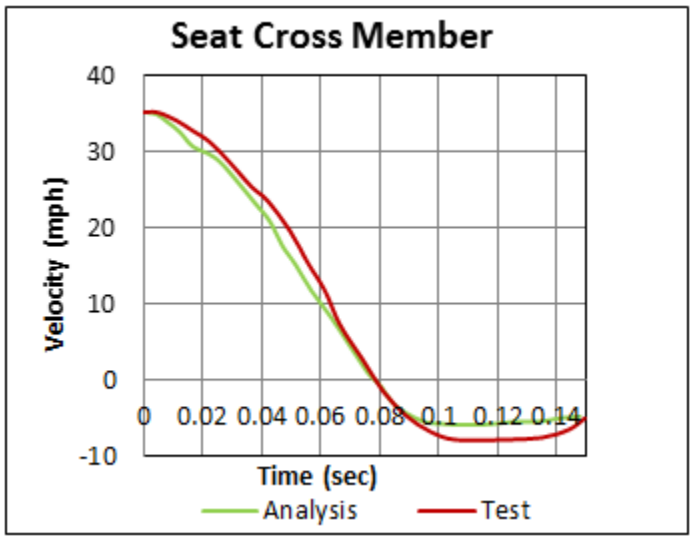

Figure 3.6: Seat cross member velocity

The FE simulation result obtained for seat cross member acceleration is also compared with the test NCAC Test 3248 in Figure 3.7. The graph obtained from the simulation is again close to the actual test result.

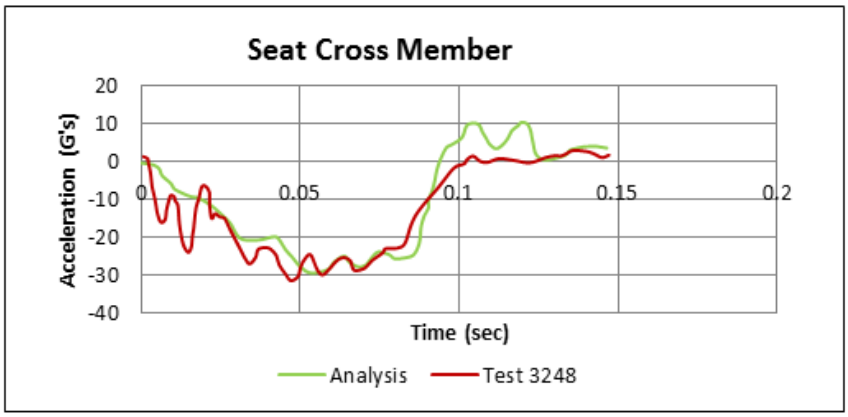

Figure 3.7: Seat cross member Acceleration

3.2.3 Validation of FE model using the Sprague and Geers Method

Using the Sprague and Geere method, the percentage of error is calculated independently in both magnitude and phase and then combined to give a comprehensive error for all validation graph [38]:

$$\text{Total Error} = \sqrt{M^2 + P^2} \tag{3.1}$$

where, M is the magnitude error, and P is the phase error, each calculated as

$$M = \sqrt{I_{sim}/I_{test}} - 1 \tag{3.2}$$

$$P = \frac{1}{\pi} cos^{-1}(I_{test\_sim} / \sqrt{I_{test} * I_{sim}}) \tag{3.3}$$

In these expressions, the variables are defined as:

$$I_{test} = \frac{1}{t_2 - t_1} \int_{t_1}^{t_2} d^2(t)\, dt \tag{3.4}$$

$$I_{sim} = \frac{1}{t_2 - t_1} \int_{t_1}^{t_2} s^2(t)\, dt \tag{3.5}$$

$$I_{test\_sim} = \frac{1}{t_2 - t_1} \int_{t_1}^{t_2} d(t)s(t)\, dt \tag{3.6}$$

where, $t_1 < t < t_2$ is evaluation period, d(t) is test/measured data, and s(t) is simulation/analysis data.

Table 3.1 shows the percentage of error obtained when comparing the graphs for validation. The overall percentage of the total error is below 20% , which is the acceptable error limit range, and hence is validated by the actual test.

Table 3.1: Sprague and Geere error calculation

Validation graph	Magnitude Error (%)	Phase Error (%)	Total Error (%)
Engine Top	-7.4	11.4	12.1
Seat Cross Member Velocity	-2.1	3.2	3.7
Seat Cross Member Acceleration	5.2	12.6	16.2

3.2.4 Car Occupant Modeling in MADYMO

The model which is developed in MADYMO is to represent a dummy positioned in a vehicle or car. The model built was similar to the model used for aircraft seat certification, with some minor changes. The bulkhead was removed and a steering representation is placed, the angle in which the steering representation was placed is similar to the angle of steering in the car.

The distance of this steering representation has been adjusted to 14, 16, and 18 inches for each set of simulation. The property that is given to the steering representation is similar to the properties given to the bulkhead, i.e, a material property for hard (steel) and soft (aluminum). The seat belt is replaced to three point seat belt and the same two properties of seat belt are used during the simulation. The details of the car occupant modeling is shown in Figure 3.8.

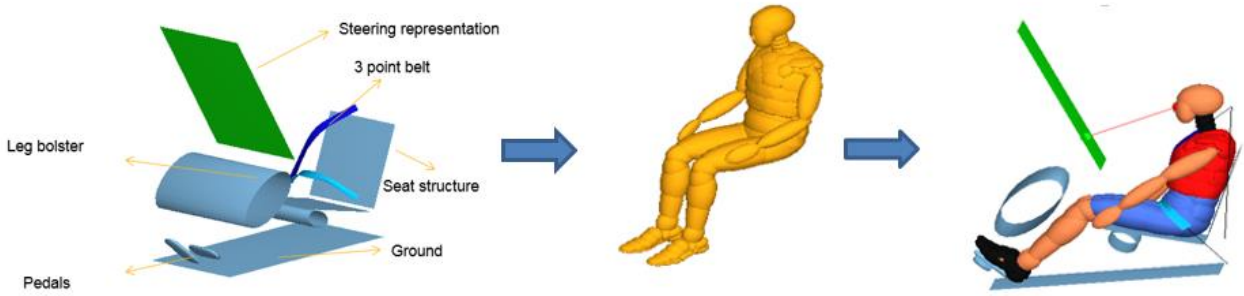

Figure 3.8: Car occupant and interior modeling representation in MADYMO

3.3 Contact Stiffness Calculations

In this study, the stiffness of the bulkhead or steering representation is given using the following equation to calculate the contact stiffness [6]:

$$K = \frac{4}{3\pi(h_i+h_j)} \left(\frac{R_i R_j}{R_i+R_j}\right)^{\frac{1}{2}} \tag{3.7}$$

where K is the contact stiffness, R_i and R_j are the radi of the bodies at the local contact zone. When the impact surface is flat, as in the case for the aircraft bulkhead or a car steering wheel frontal surface, the contact stiffness reduces to

$$K = \frac{4\sqrt{R_H}}{3\pi(h_H + h_S)} \tag{3.8}$$

where *S* denotes the impact surface, *H* denotes the Head, and here R_H is the Radius of ATD head. The material constants are calculated as

$$h_H = \frac{1 - {v_H}^2}{\pi\, E_H} \qquad\qquad h_S = \frac{1 - {v_S}^2}{\pi\, E_S} \tag{3.9}$$

Here, the v is the Poisson's ratio, and E is the Young's modulus for each of the impacting bodies. Figure 3.9 shows a sample representation of head and impact surface. Using the stiffness Equations (3.8) and (3.9), the contact stiffness value calculated for the aluminum becomes 6.99×10^5 N/m$^{1.5}$, and for the steel it becomes 3.45×10^5 N/m$^{1.5}$.

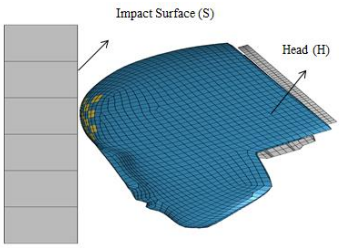

Figure 3.9: Sample representation of head and impact surface

3.4 Simulations of Head Impacts

3.4.1 Aircraft Interior Head Impacts

The simulations for testing the occupant response in actual aircraft is done using the MADYMO. As discussed earlier, the acceleration test pulse obtain for Part 23 pilot, Passenger and Part 25 is applied to the MADYMO occupant model for the simulations and repeated for various sets of parameter such as belt type (nylon, polyester and without belt), seat pitch (32", 35" and 38") and bulkhead stiffness (steel and aluminum). Figure 3.10 shows sequence of simulation motion for the aircraft occupant model with and without the belt. As observed, the belt provides some protection for the occpants, but a head impact to the frontal structure is typically obliqued at an angle, larger than the case for the no-belt configuration.

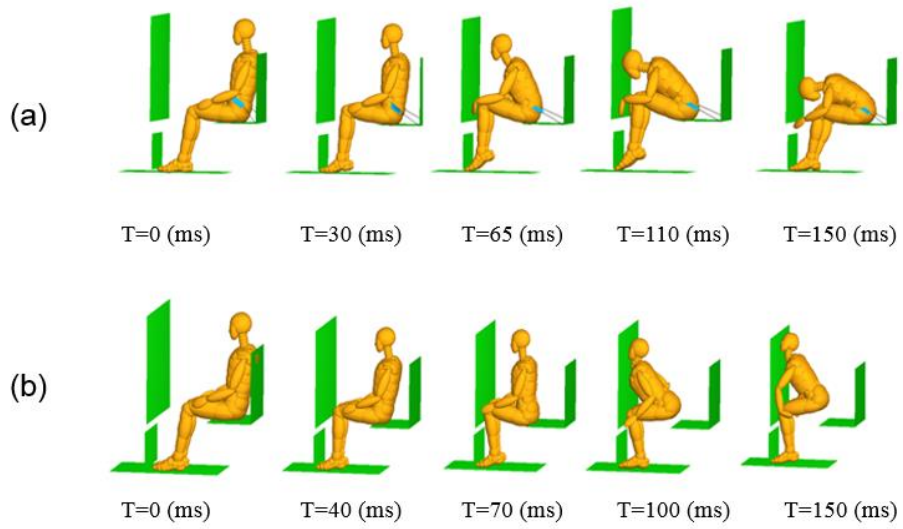

Figure 3.10: Animation sequence for MADYMO simulation model, with (a) simulation with a lap belt and (b) without a belt.

3.4.2 Automotive Interior Head Impacts

After the simulation, the acceleration pulse generated in the driver's seat due to crash is measured and imported into the MADYMO model. Using this acceleration pulse the MADYMO simulation is done for automotive frontal impact scenarios. The simulation is repeated for different set of parameter such as belt type, different distances between dummy head and impact surface and impact surface material. Figure 3.11 shows the sample animation sequence of the MADYMO model for automotive.

Figure 3.11: MADYMO model animation sequence for automotive

CHAPTER 4

RESULTS AND DISCUSSIONS

4.1 HIC Evaluation

For each set of occupant head impact in aircraft and automotive scenarios, 3 different output values are measured, namely, the head impact velocity, the head impact angle and the HIC. Among the three output results, the HIC is the most significant one. In MADYMO, the HIC value is calculated in the post processor using the injury option for the resultant acceleration curve obtain from the simulation. For each set of parameters and crash scenario, the HIC value is calculated in this study. Figure 4.1 shows a sample plot for HIC for head resultant acceleration in G's, with the peak acceleration of 190 G's. The HIC for this sample is calculated to be 1614, and related parameters are t_1=74 ms, t_2=108 ms, t_2-t_1=34 ms recorded for the sample plot.

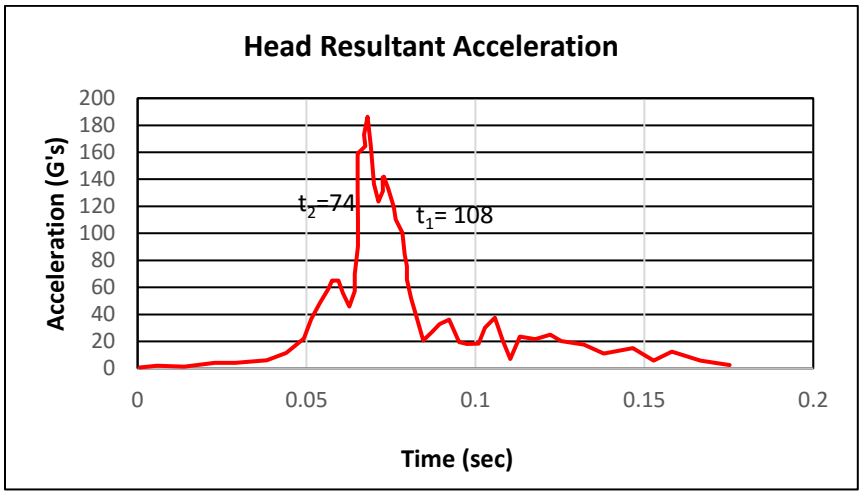

Figure 4.1: Sample head resultant acceleration plot

4.2 Head Impact Velocity Evaluation

The velocity at which the head impacts on the impact surface for aircraft and automotive is also calculated in the MADpost using the special function to calculate the resultant from two

curves [39]. The head impact velocity is calculated for each set of parameters and for different crash scenarios for both aircraft and automotive input data. The complete set of results obtained is shown in the Tables 4.1 through 4.4. Figure 4.2 represents a sample head impact velocity plot.

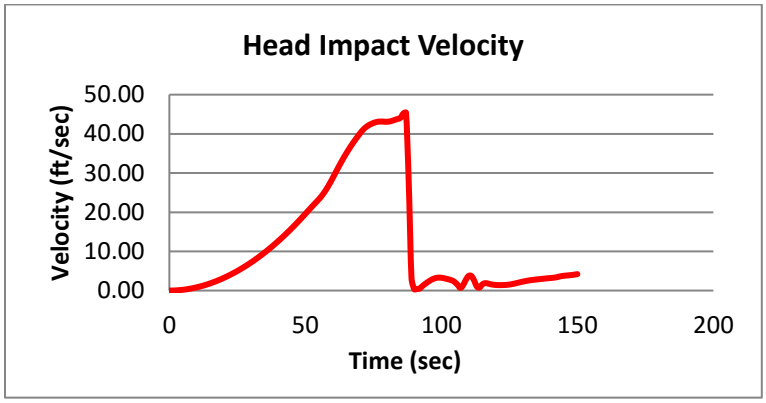

Figure 4.2: Head impact velocity plot

4.3 Head Impact Angle Evaluation

The head impact angle is calculated using the head path profile, as shown for the sample head path in Figure 4.3 (a). The outline of the head profile is shown on the graph to illustrate how the head travels and impacts the impact surface. The path of head is obtained by plotting the head displacement output file for the vertical motion Z versus the longitudinal motion X.

Figure 4.3(b) is the representation of head and bulkhead model or the impact surface model, to show how the head impact angle is calculated when head is impacted. From the point of impact, a tangent line is drawn and the corresponding angle is calculated by tracing the head path after the impact surface. The impact angle is calculated for each set of impact parameters and for the different crash scenarios.

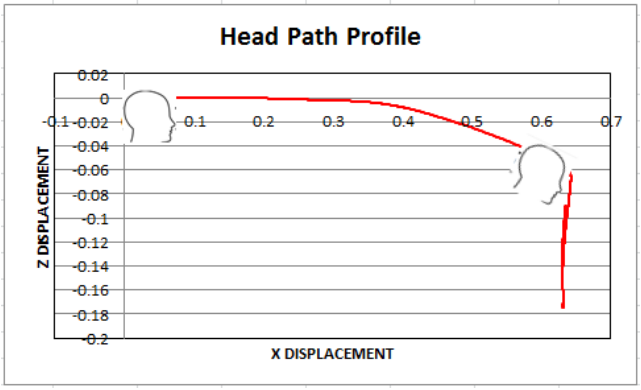

Figure 4.3(a): Methods for calculating the Head impact graph

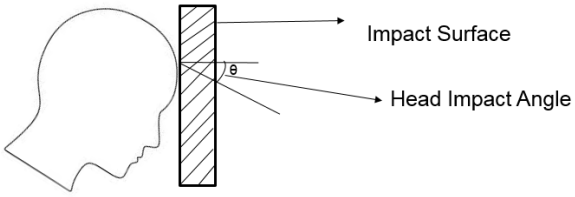

Figure 4.3(a): Head profile for calculating the Head impact angle

4.4 Acceleration Pulse at the Car Driver Seat

For the automotive head impact simulations, the MADYMO program needs certain input data for the simulation. The acceleration pulse obtained from the driver's seat of Ford Taurus is used as the input. Figure 4.4 shows the acceleration pulse obtained from the driver's seat.

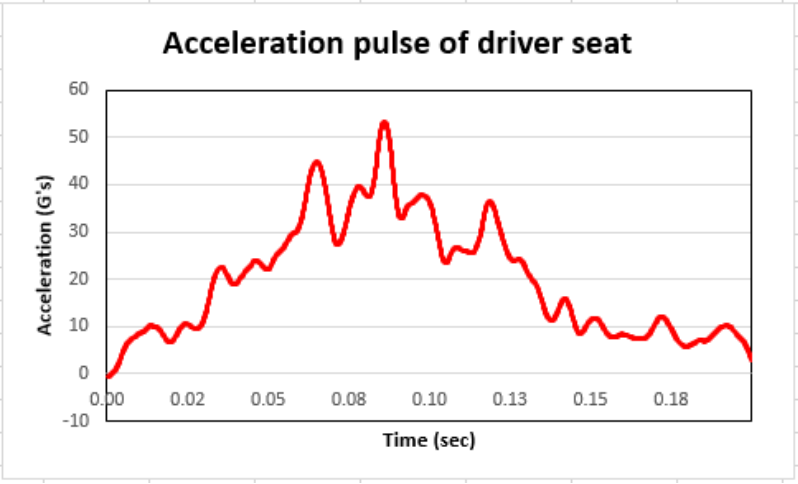

Figure 4.4: Acceleration pulse at the car driver's seat

To model and simulate occupant responses in different crash scenarios, the MADYMO program needs certain input data for the simulation. The triangular input acceleration pulse of section 1.4 for aircraft conditions and using the acceleration pulse obtained from the driver's seat for the automotive condition, simulations are carried for different parameters, such as bulkhead or impact surface stiffness and belt material and the seat pitch distances (32", 35" and 38" for aircraft and 14", 16" and 18" for automotive). The complete matrix of simulation test results for the Part 23 Pilot, Passenger, and Part 25, and automotive is shown in Tables 4.2 through 4.5.

4.5 HIC Results for Aircraft and Automotive Head Impacts

4.5.1 Part 23 Pilot Head Impact Results

Table 4.1 shows the results obtained for the Part 23 pilot test condition. The complete results obtained for different belt material, seat pitch distances and bulkhead material is shown.

Table 4.1: Results for Part 23 pilot

Aviation- Run-1	FAR 23 PILOT	Bulkhead material	Belt Material	velocity (ft/sec) and Impact angle (degree) for Seat pitch							
				32		35		38			
				V	ϴ	V	ϴ	V	ϴ		
		Hard	Nylon	47.1	32.4	49.1	34.1	39.3	36.2		
			Polyester	44.3	31.3	46.6	35.3	36.2	39.3		
			No belt	60.3	—	62.5	—	64	—		
Aviation- Run-2	FAR 23 PILOT	Bulkhead material	Belt Material	HIC for Seat pitch							
				32		35		38			
		Hard	Nylon	3215		2891		1864			
			Polyester	2836		1896		1212			
			No belt	4016		4234		4450			
Aviation- Run-3	FAR 23 PILOT	Bulkhead material	Belt Material	HIC for Seat pitch							
				32		35		38			
		Soft	Nylon	2936		2651		1561			
			Polyester	2547		1650		927			
			No belt	3570		3714		3869			

4.5.2 Part 23 Passenger Head Impact results

Table 4.2 shows the results obtained for Part 23 passenger. The complete matrix of results obtained for different belt material, seat pitch distances and bulkhead material steel (hard) and aluminum (soft) are shown.

Table 4.2: Results for Part 23 passenger

Aviation- Run-4	FAR 23 PASSANGER	Bulkhead material	Belt Material	velocity (ft/sec) and Impact angle (Theta) for Seat pitch							
				32		35		38			
				V	ϴ	V	ϴ	V	ϴ		
		Hard	Nylon	44.4	32.2	49.1	37.8	42.3	44.4		
			Polyester	39.5	34.4	43.5	36.6	29.8	42.1		
			No belt	58.2	_	60.6	_	61.1	_		
Aviation- Run-5	FAR 23 PASSANGER	Bulkhead material	Belt Material	HIC for Seat pitch 32		35		38			
		Hard	Nylon	2224		1721		1399			
			Polyester	1627		1208		899			
			No belt	3009		3185		3297			
Aviation- Run-6	FAR 23 PASSANGER	Bulkhead material	Belt Material	HIC for Seat pitch 32		35		38			
		Soft	Nylon	2120		1684		1361			
			Polyester	1580		1157		816			
			No belt	2911		3006		3194			

4.5.3 Part 25 Head Impact Results

Table 4.3 shows the results obtained for Part 25 . The complete matrix of results obtained for different belt material, seat pitch distances and bulkhead material is shown in the Table 4.3. The HIC results obtained for Part 25 is observed to be higher than the one corresponding to the for Part 23 pilot and passenger conditions. When polyester belt is utilized the HIC results are under the permissible threshold of 1000

Table 4.3: Results for Part 25

Aviation- Run-7	FAR 25	Bulkhead material	Belt Material	velocity (ft/sec) and Impact angle (Theta) for Seat pitch							
				32		35		38			
				V	Θ	V	Θ	V	Θ		
		Hard	Nylon	32.3	28.3	35.5	35.4	29.1	44.2		
			Polyester	27.6	30.2	31.6	39.2	27.3	43.5		
			No belt	45.2	_	47.6	_	49.2	_		
Aviation- Run-8	FAR 25	Bulkhead material	Belt Material	HIC for Seat pitch 32		35		38			
		Hard	Nylon	1361		1242		926			
			Polyester	931		841		763			
			No belt	1944		2029		2198			
Aviation- Run-9	FAR 25	Bulkhead material	Belt Material	HIC for Seat pitch 32		35		38			
		soft	Nylon	1320		1242		900			
			Polyester	910		827		741			
			No belt	1896		1998		2012			

4.5.4 Automotive Head Impact Results

Using the acceleration pulse obtained from the driver's seat for automotive, simulations are carried for different parameters such as steering representation stiffness (steel and aluminum), belt material (polyester and nylon) and the distance between the dummy head and steering representation (14", 16" and 18"). Table 4.4 shows the results obtained for automotive head impact. The complete matrix of results obtained for different belt material, distances is shown.

Table 4.4: Results for Automotive head impact

Automotive-run-13	3 point belt	Steering Representation Material	Belt Material	Impact velocity (ft/sec) for distances		
				14	16	18
		Hard	Nylon	33.3	37.1	30
			Polyester	31.6	34.7	28.2
Automotive-run-14	3 point belt	Steering Representation Material	Belt Material	Impact angle (degree) for distances		
				14	16	18
		Hard	Nylon	75.2	83.5	90.2
			Polyester	73.6	81.4	87.2
Automotive-run- 15	3 point belt	Steering Representation Material	Belt Material	HIC for distances		
				14	16	18
		Hard	Nylon	1527	1621	1201
			Polyester	1414	1575	1147
Automotive-run-16	3 point belt	Steering Representation Material	Belt Material	HIC for distances		
				14	16	18
		Soft	Nylon	1274	1410	1104
			Polyester	1236	1324	960

4.6 Variations of HIC, Impact Angle, and Impact Velocity with Seat Pitch

In order to understand the results obtained for Part 23 Pilot, Passenger, Part 25 and automotive, scattered graphs are plotted for the results obtained using the belt material nylon, polyester, and without a belt. The graphs are plotted between the seat pitch distances 32”, 35” and 38” versus the output results HIC, impact angle and impact velocity. For the aircraft head impact model results, the scattered graph shows that the HIC value and head impact velocity decreaseS with THE increase in seat pitch distances from 32” to 38” for the nylon and polyester belt material. Whereas, the impact angle increases with the increase in seat pitch distances. Similarly, for the automotive head impact model results, the scattered graph obtained for the HIC, impact angle, and impact velocity follow the same pattern as the aircraft head impact model results.

4.6.1 Aircraft Head Impact Data Plots

Figures 4.5 and 4.6 represent the Part 23 Pilot HIC variations with the seat pitch of 32" 35" and 38", for the aluminum and steel bulkheads. The graphs are plotted to show how the HIC value decreases with increase in seat pitch for the different belt material and for without a belt, the HIC is nearly same. The HIC value are all quite large except for the larger seat pitch distance and the use of polyester seat belt for aluminum bulkhead, which is under the permissible limit as the head only glances the bulkhead. We can also observe that the HIC values obtained for the polyester belt is slightly less when compared to the nylon belt case.

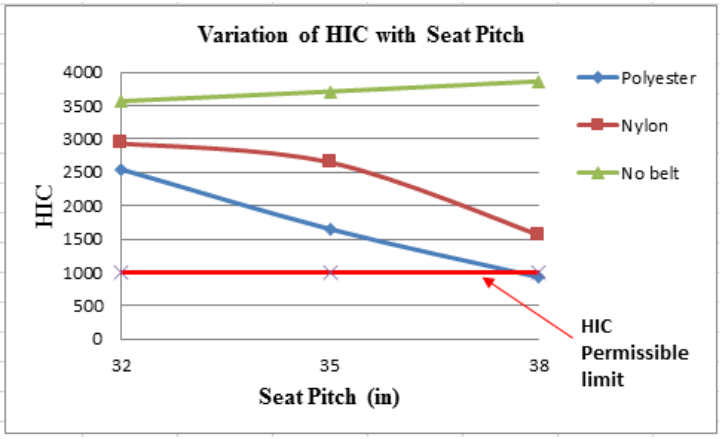

Figure 4.5: HIC values for Part 23 pilot with seat pitch for aluminum bulkhead

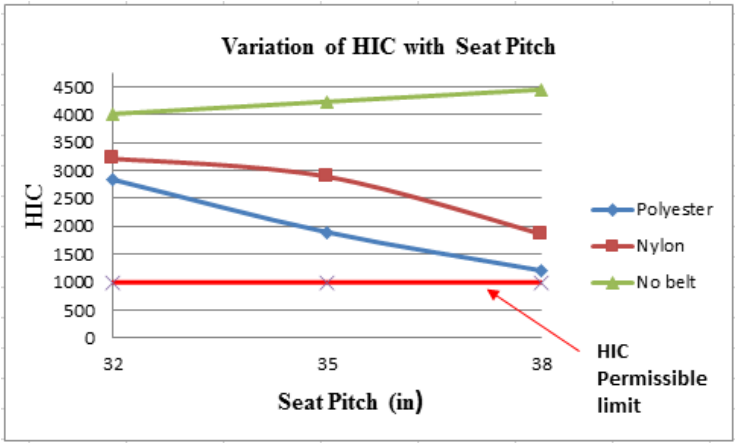

Figure 4.6: HIC values for Part 23 pilot with seat pitch for steel bulkhead

Figures 4.7 and 4.8 represent the Part 23 Pilot impact angle and impact velocity variation with seat pitch 32" 35" and 38". The graphs are plotted to show how the impact angle and velocity is varied with the increase in seat pitch for the polyester and nylon belts. With an increase in seat pitch distances, the impact angle is increased for both belt material. Whereas, the impact velocity is less for the largest seat pitch distance for both belt type material and for without belt, the impact velocity is almost same for different seat pitch distances.

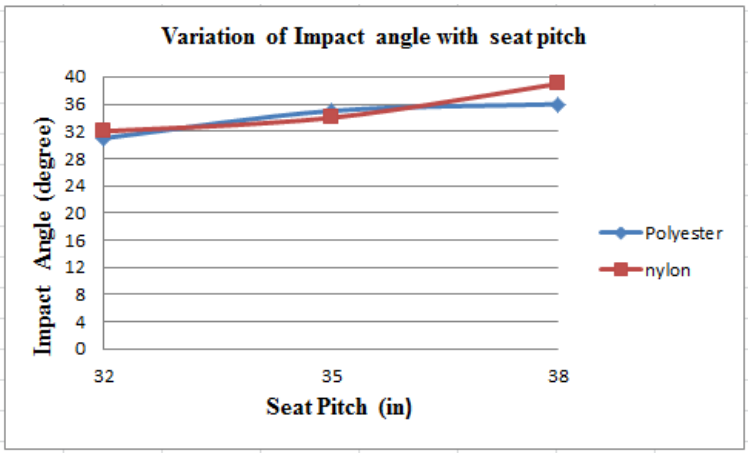

Figure 4.7: Impact angle variation for Part 23 pilot with seat pitch

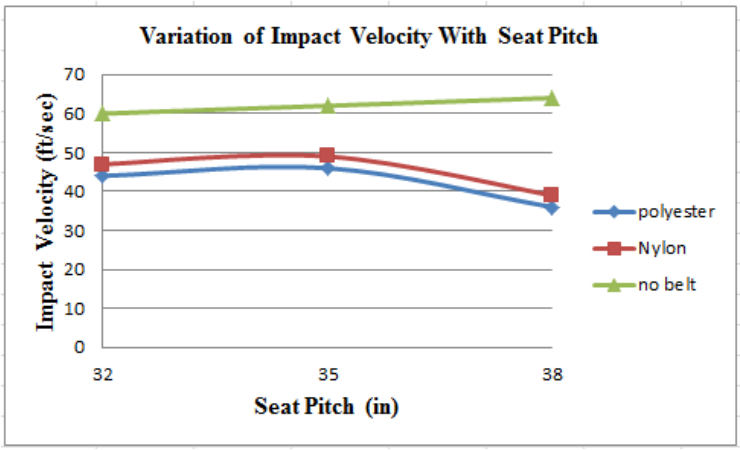

Figure 4.8: impact velocity variation for Part 23 pilot with seat pitch

Figures 4.9 and 4.10 represent the Part 23 Passenger HIC variations with the seat pitch of 32” 35” and 38”, for the aluminum and steel bulkheads. The graphs are plotted to show how the HIC value decreases with increase in seat pitch for the different belt material and for without a belt, the HIC is nearly the same. The HIC value are all quite large except for the larger seat pitch distance and use of polyester seat belt for aluminum bulkhead, which is under the permissible limit as the head only glances the bulkhead. We can also observe that the HIC values obtained for the polyester belt is slightly less when compared to the nylon belt case.

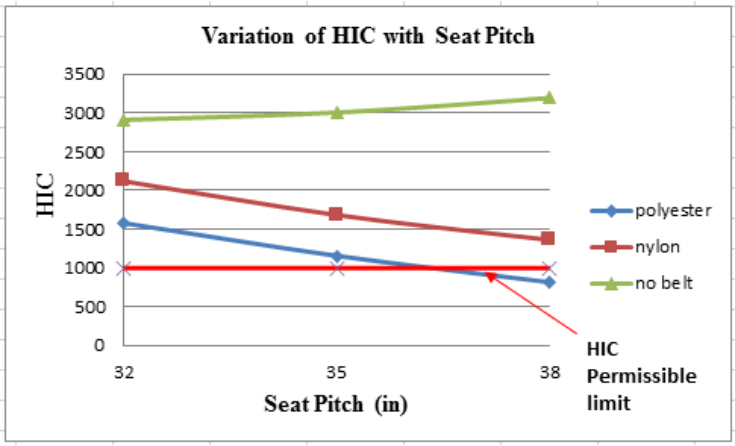

Figure 4.9: HIC variations for Part 23 passenger with seat pitch for aluminum aulkhead

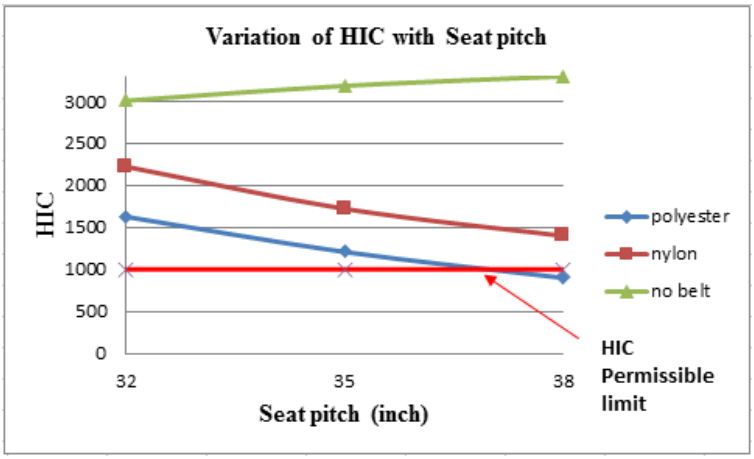

Figure 4.10: HIC variation for Part 23 passenger with seat pitch for steel bulkhead.

Figures 4.11 and 4.12 represent the Part 23 Pilot impact angle and impact velocity variation with seat pitch 32" 35" and 38". The graphs are plotted to show how the impact angle and velocity is varied with increase in seat pitch for polyester and nylon belt. With an increase in seat pitch distances, the impact angle is increased for both the belt material. Whereas, the impact velocity is less for the largest seat pitch distance for both the belt material and for without belt the impact velocity is almost the same for different seat pitch distances.

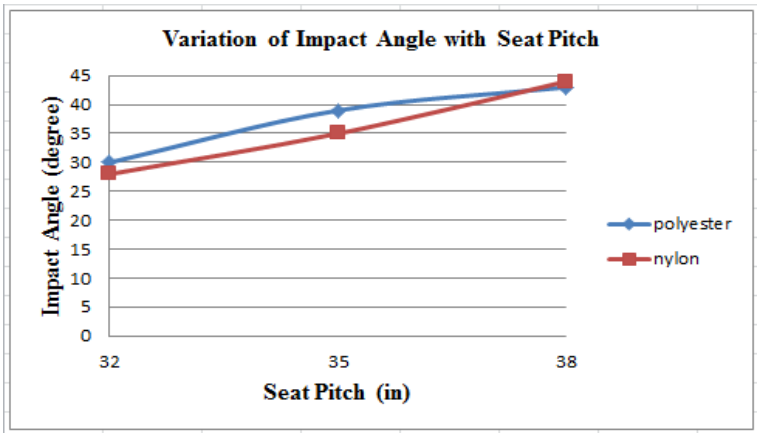

Figure 4.11: Impact angle variations for Part 23 passenger with seat pitch

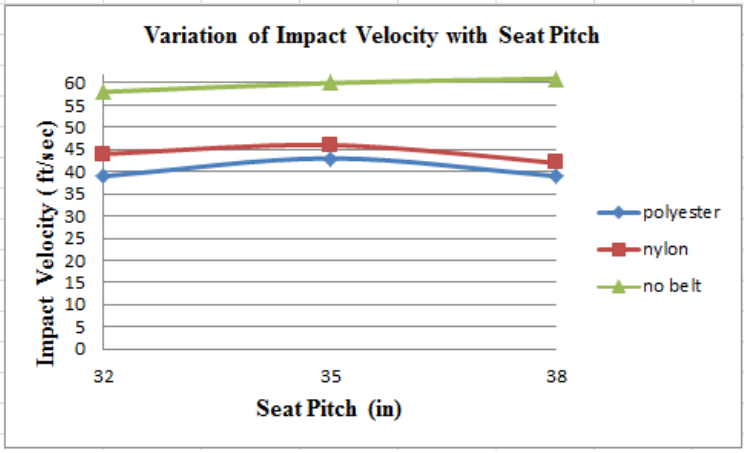

Figure 4.12: Impact velocity variations for Part 23 passenger with seat pitch

Figures 4.13 and 4.14 represent the Part 25 HIC variations with the seat pitch of 32" 35" and 38", for the aluminum and steel bulkheads. The graphs are plotted to show how the HIC value decreases with increase in seat pitch for the different belt material and for without a belt, the HIC is nearly same. The HIC value are under the permissible limit for all the seat pitch distances for the polyester seat belt. Whereas, for the use of nylon belt, the HIC value are all quite large except for the larger seat pitch distance for the aluminum and steel bulkheads.

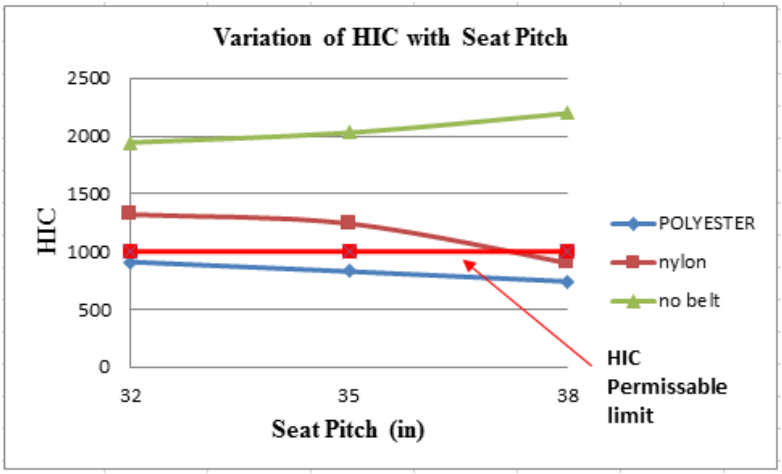

Figure 4.13: HIC variation for Part 25 with seat pitch for aluminum bulkhead

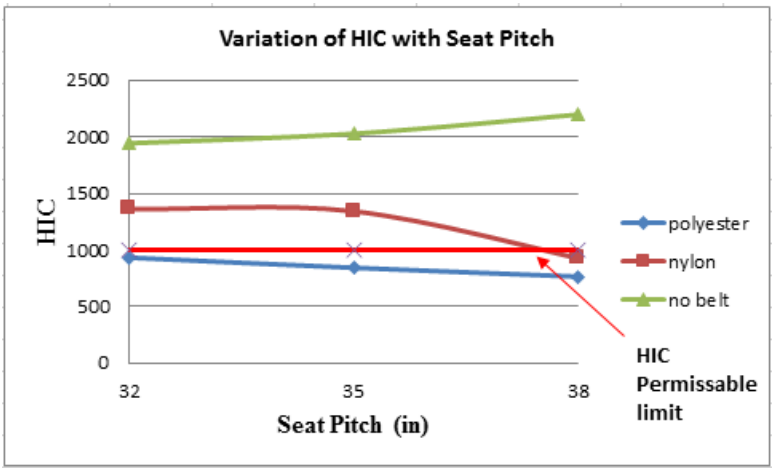

Figure 4.14: HIC variation for Part 25 with seat pitch for steel bulkhead

Figures 4.15 and 4.16 represent the Part 25 impact angle and impact velocity variations with seat pitch 32" 35" and 38". The graphs are plotted to show how the impact angle and velocity are varied with the increase in seat pitch for polyester and nylon belt. With an increase in seat pitch distances, the impact angle is increased for both the belt materials. Whereas, the impact velocity is less for the largest seat pitch distance for both the belt material, and for without belt the impact velocity increases with increase in seat pitch distances.

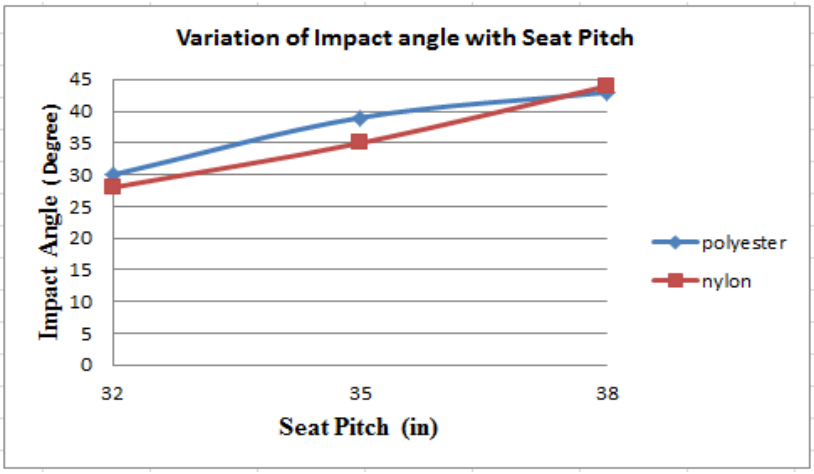

Figure 4.15: Impact angle variations for Part 25 with seat pitch

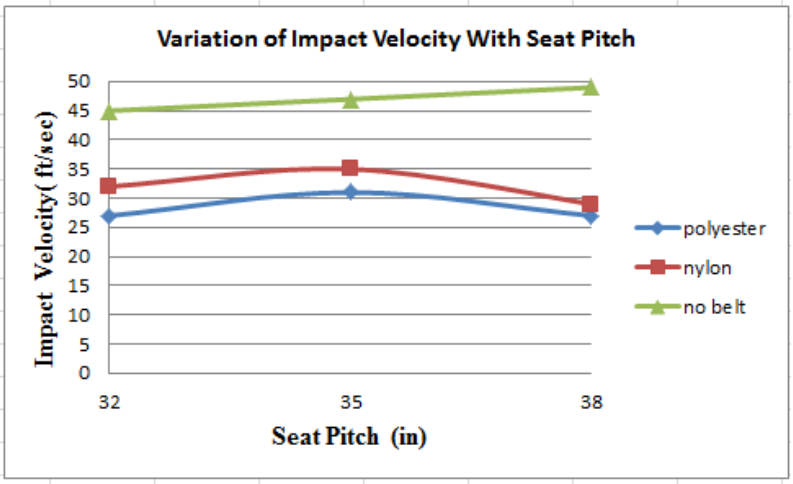

Figure 4.16: Impact velocity Variations for Part 25 with seat pitch

Figures 4.17 and 4.18 represent the HIC variations for the Part 23 pilot, passenger and Part 25 with pitch 32", 35" and 38" for aluminum and steel bulkheads. The graphs are plotted show how the HIC value decreases with the increase in seat pitch for various crash scenarios in aircraft in one combine plot using polyester and nylon belt type. Overall, for larger seat pitch distance, the HIC value is under the permissible limit for Part 23 Pilot and Passenger. Whereas, for Part 25 using polyester, the HIC value is under the permissible limit for all seat pitch distances for both aluminum and steel bulkhead.

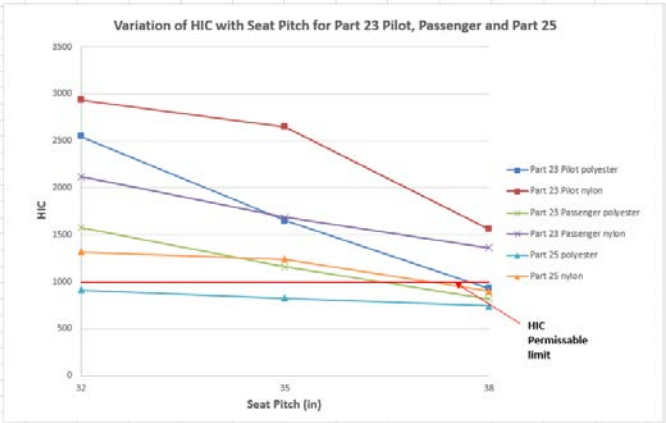

Figure 4.17: HIC combine plot for aluminum bulkhead for Part 23 pilot, passenger and Part 25

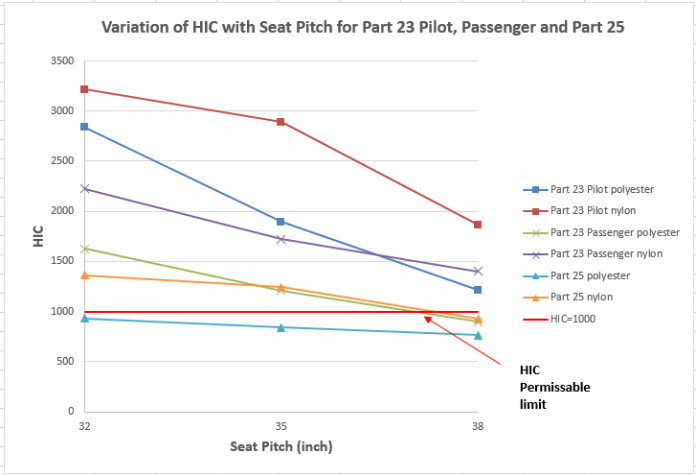

Figure 4.18: HIC combine plot for steel bulkhead for Part 23 pilot, passenger and Part 25

Figures 4.19 and 4.20 represent variations of impact angle and velocity for Part 23 pilot, passenger and Part 25 with pitch of 32", 35" and 38". The graphs are plotted show how the angle and velocity are varied for various crash scenarios in aircraft in one combine plot using polyester and nylon belt type. The impact angle is maximum for the large seat pitch distance and impact velocity is maximum for the seat pitch distance of 35-in for all crash scenarios.

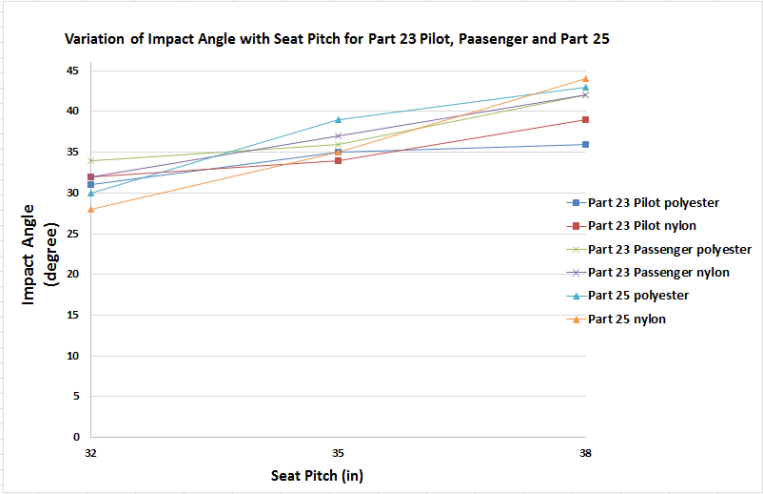

Figure 4.19: Impact angle combined plot for steel bulkhead for Part 23 pilot, passenger and Part 25 with seat pitch

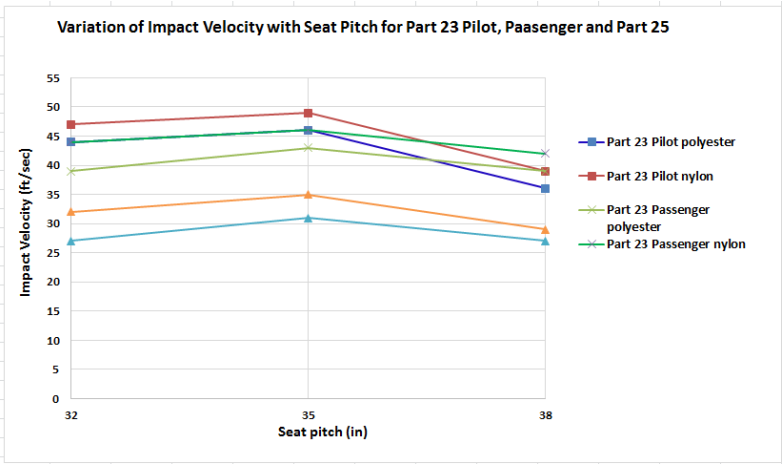

Figure 4.20: Impact velocity combined plot for steel bulkhead for Part 23 pilot, passenger and Part 25 with seat pitch

4.6.2 Automotive Head Impact Data Plots

Figures 4.21 and 4.22 represent the HIC variations for the automotive case with different distances between the dummy head and steering representation with steel and aluminum materials. The graph is plotted to show how the HIC value is varied with an increase in the distances using polyester and nylon belt. Overall, the HIC values are smaller for automotive than the ones obtain for aircraft, because of the lower input of accelerations and the use of the 3-point belt. The least HIC value is obtained for the dummy head to impact surface distance of 18-in using the polyester belt materials.

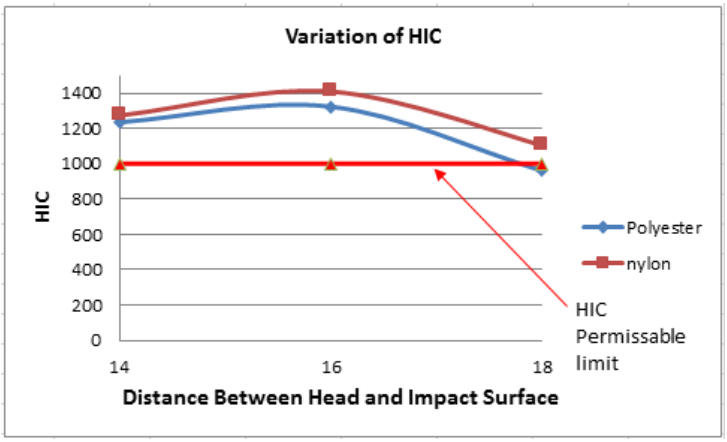

Figure 4.21: HIC variations for automotive inputs – aluminum

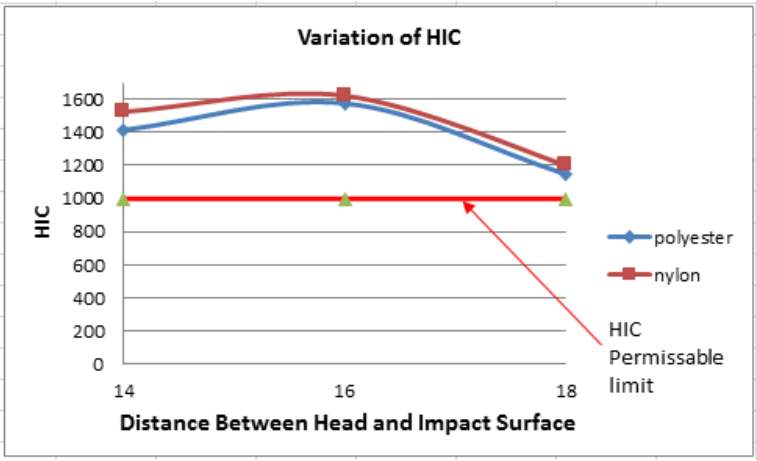

Figure 4.22: HIC variations for automotive inputs – steel

Figures 4.23 and 4.24 represent the impact angle and impact velocity variations for the automotive case with different distances between the dummy head and the steering representation material steel. The impact angle increases with an increase in distance and its nearly the same for the belt nylon and polyester materials. The impact velocity is maximum for the head to impact surface distance of 16-in for the nylon and polyester belt material.

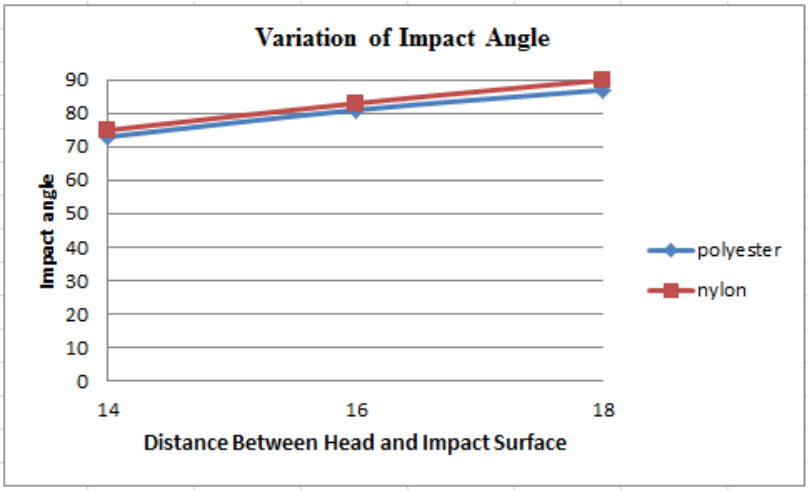

Figure 4.23: Impact angle variations for automotive inputs

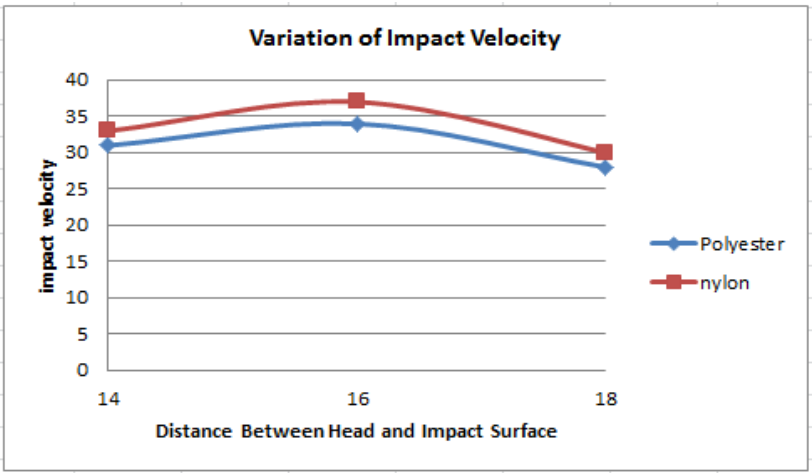

Figure 4.24: Impact angle variations for automotive inputs

CHAPTER 5

RESPONSE SURFACES USING DESIGN-OF-EXPERIMENTS/KRIGING MODEL

5.1 Design-of-Experiments

A computational experiment is utilized to study and understand the various factors affecting the HIC by developing a response surface data obtained from the results. Initially, the design points are selected to obtain the performance data from the MADYMO simulations. Each computer simulation has a set of design parameters for which a set of results are obtained. Using these design points or results, a Kriging model is built. The main objective of this is to optimize the results and to develop a prediction model for any given design points using the Kriging model to help in reducing the number of computer simulations as well as optimal design configuration. Implementation of this method is shown in Figure 5.1, which illustrates the flow chart representation of the DOE/Kriging process.

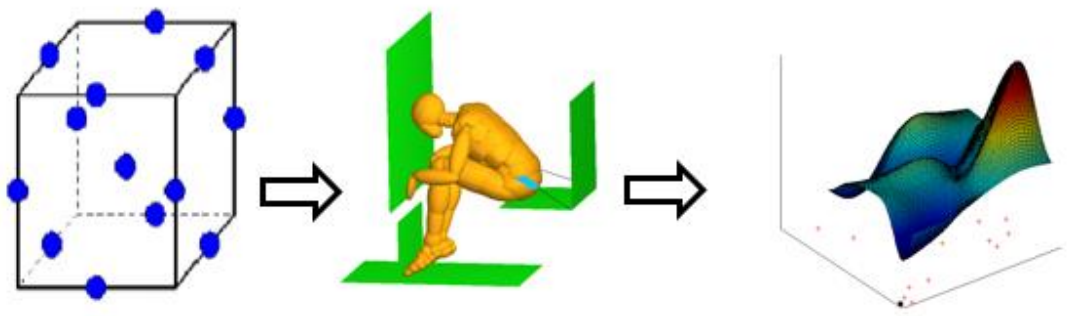

Sample Input Data Computer Simulation Model (MADYMO) Kriging Model

Figure 5.1: Flowchart representation of DOE/Kriging process

5.2 Kriging Model

Kriging model is built using the multi-objective optimization method to interpolate the given set of sample points to a model approximately [12].

A Kriging model to estimate the unknown function y (x) can be expressed as

$$Y(x) = \mu + Z(x) \tag{5.1}$$

where x is m-dimensional vector, Y(x) is the unknown function, μ is the constant global model and Z(x) is the realization of a Gaussian stochastic process which represents the local deviation from the global model. The correlation for the Z(x) matrix can be given by

$$Corr[Z(x_i , x_j)] = \sigma^2 \ d(x_i , x_j) \tag{5.2}$$

where the distance between the two sample point's x_i and x_j can be expressed as follows

$$d(x_i , x_j) = -\left[\exp \ \ \sum_{k=1}^{m} \theta_k |x_k^i - x_k^j|^2 \right] \tag{5.3}$$

where θ_k is the k_{th} element of the correlation vector and term inside the exponential is the distance between the two sample point x_i, x_j . With n sample point the like hood function of model parameters can be given by:

$$Likelihood = -\frac{n}{2} ln(2\pi) - \frac{n}{2} ln\, \sigma^2 - \frac{1}{2} ln \left| R \right| - \frac{1}{2\sigma^2} (y-A\mu)^T R^{-1} (y- A\mu) \tag{5.4}$$

where *y* is the column vector response, *A* denotes the m dimensional unit vector, R denotes the n × m matrix whose *(i, j)* entry is Corr[Z(x_i , x_j)]. The parameters μ and σ^2 can be defined as

$$\mu = [A^t \ R^{-1} Y]^{-1} A^t \ R^{-1} y \tag{5.5}$$

The σ^2 can be estimated as:

$$\sigma^2 = \frac{(y-A\mu)^t \ R^{-1} (y-A\mu)}{n} \tag{5.6}$$

Using the two Equations (5.5) and (5.6), the likehood function can be transformed and maximized. Therefore, correlation matrix R can be calculated. The Kriging predictive model is given by

$$y(x^*) = \mu + r^t(x^*)R^{-1}(y\text{-}A\mu) \tag{5.7}$$

which can be used to predict the model response at a different set of output values.

5.3 Input and Output Parameters for Surface Plots

Using the results obtained from the MADYMO simulations for the given set of design variables, a surface plot is generated. Table 5.1 shows the list of input and output data used in plotting the surface plot. The surface plot is used to represent the results obtained and to understand how the results are varied for the given set of design variable. The surface plot contains 3 axis; i.e, x, y and z axis, with x-axis and y-axis common for all the plot representing seat pitch distances and belt material and the z-axis represents the output data; i.e., the head impact angle, head impact velocity, and the HIC as shown in Table 5.1. A total of 6 data points is used in each plot to obtain the response surface.

Table 5.1: Input and output parameters used for surface plot generation.

Input Parameters:	Seat Pitch Distances: (aircraft) 32", 35", 38"	Head to Steering Distances: (automotive) 14", 16" and 18"	Belt Type Material Nylon, Polyester
Output Parameters:	HIC Head Impact Angle (degree) Head Impact Velocity (ft/sec)		

5.4 Surface Plots for Aircraft Head Impacts

5.4.1 Surface Plots for Part 23 Pilot

Figures 5.2 and 5.3 are the surface plots of the HIC for the aluminum and steel bulkheads for Part 23 Pilot. From the plots, we can observe that the HIC value decreases with the increase in seat pitch distances, for the belt material nylon and polyester, for both aluminum and steel bulkheads. We can also observed that the HIC values obtained for the polyester belt are slightly lower when compared to the nylon belt and the best permissible HIC value obtained is for the seat pitch distance of 38-in for the aluminum bulkhead, using the polyester belt.

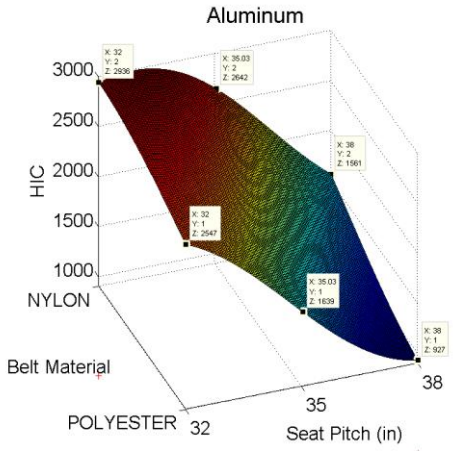

Figure 5.2: Surface plot of HIC for aluminum bulkhead for Part 23 pilot

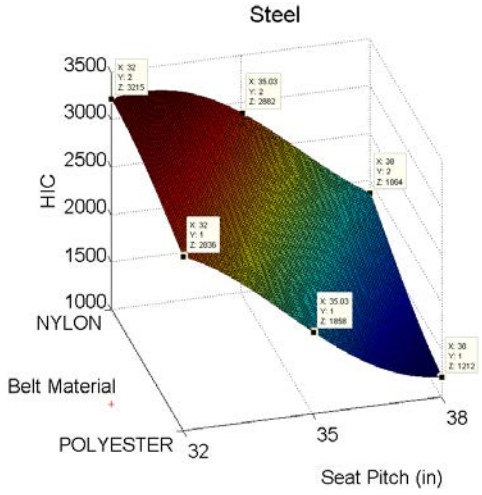

Figure 5.3: Surface plot of HIC for steel bulkhead for Part 23 pilot

Figures 5.4 and 5.5 are the surface plots of the head impact angle and head impact velocity for Part 23 Pilot. From the plots we can observe that the head impact angle increases with the increase in seat pitch distances for both belt materials of nylon and polyester. Similarly, for the head impact velocity, we can observe that the impact velocity is least for the seat pitch distance 38-in and highest for the seat pitch distance 35-in.

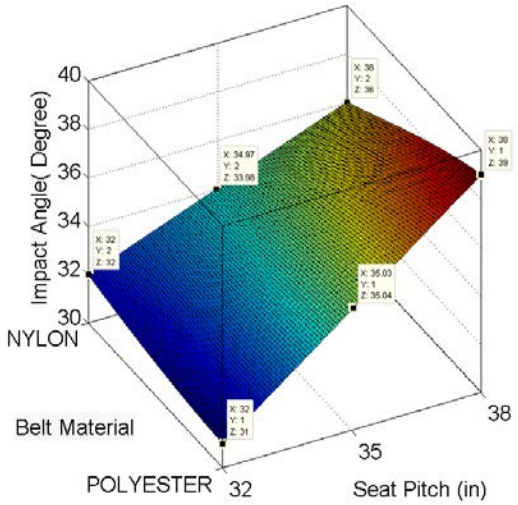

Figure 5.4: Surface plot of head impact angle for Part 23 pilot

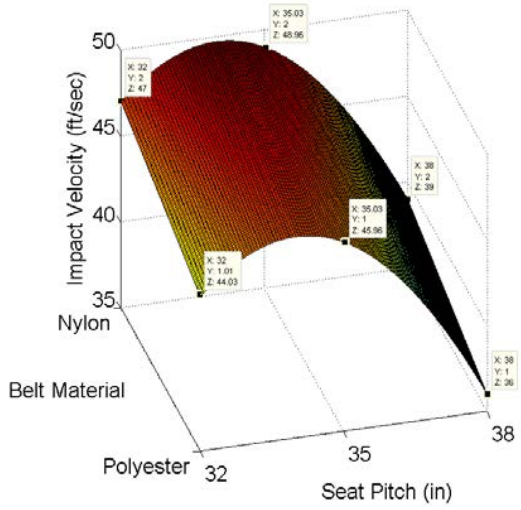

Figure 5.5: Surface plot of head impact velocity for Part 23 pilot

5.4.2 Surface Plots for Part 23 Passenger

Figures 5.6 and 5.7 are the surface plots of the HIC for the aluminum and steel bulkheads for Part 23 Passenger. From the plots we can observe that the HIC value decreases with the increase in seat pitch distances, for the belt material of nylon and polyester, for both aluminum and steel bulkheads. We can also observed that the HIC values obtained for polyester belt are slightly lower when compared to the nylon belt. The best permissible HIC value obtained is for the seat pitch distance 38-in for both aluminum and steel bulkheads, using the polyester belt.

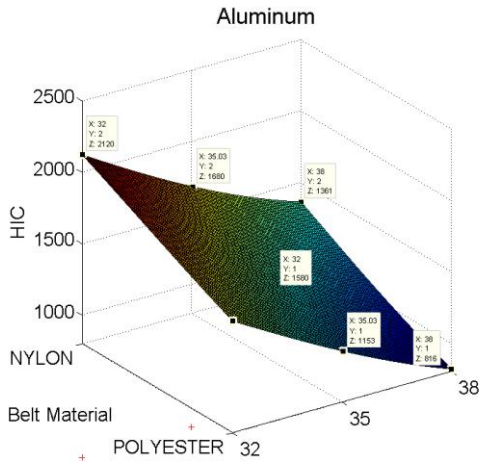

Figure 5.6: Surface plot of HIC for aluminum bulkhead for Part 23 passenger

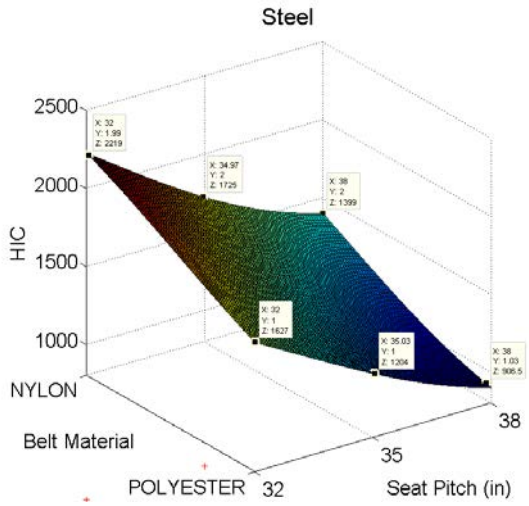

Figure 5.7: Surface plot of HIC for steel bulkhead for Part 23 passenger

Figures 5.8 and 5.9 are the surface plots of the head impact angle and head impact velocity for Part 23 Passenger. From the plots we can observe that the head impact angle increases with the increase in seat pitch distances for the belt materials of nylon and polyester. Similarly, for the head impact velocity, we can observe that the impact velocity is least for the seat pitch distance 38-in and highest for the seat pitch distance 35-in.

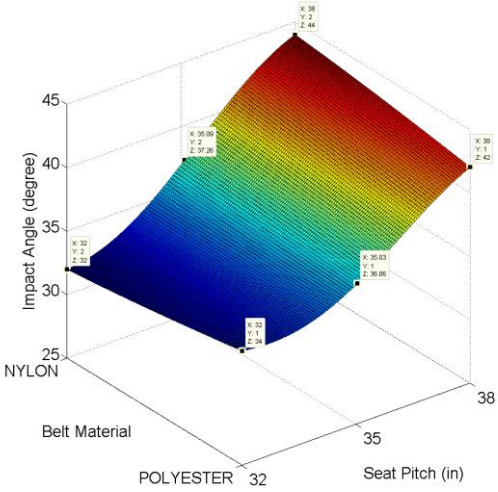

Figure 5.8: Surface plot of head impact angle for Part 23 passenger

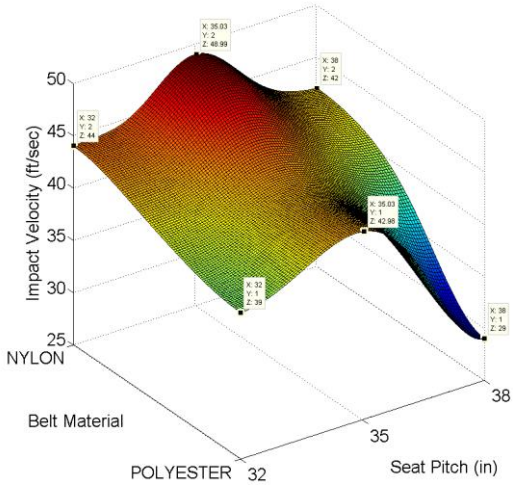

Figure 5.9: Surface plot of head impact velocity for Part 23 passenger

5.4.3 Surface Plots for Part 25

Figures 5.10 and 5.11 are the surface plots of HIC for aluminum and steel bulkheads for Part 25. From the plots we can observe that the HIC value decreases with the increase in seat pitch distances, for the belt materials of nylon and polyester, for both aluminum and steel bulkheads. We can also observed that the HIC values obtained for the polyester belt are slightly lower when compared to the nylon belt. The best permissible HIC value is obtained for the all the three seat pitch distances for the aluminum bulkhead, and using the polyester belt.

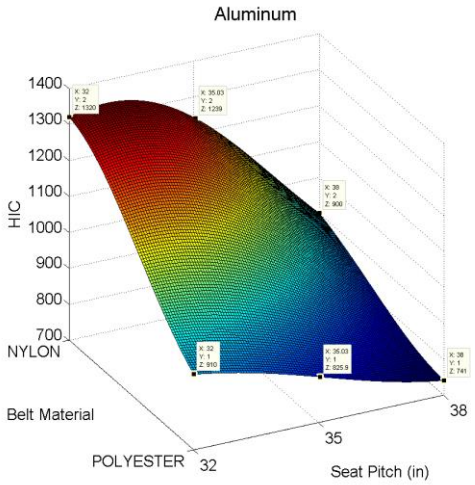

Figure 5.10: Surface plot of HIC for aluminum bulkhead for Part 25

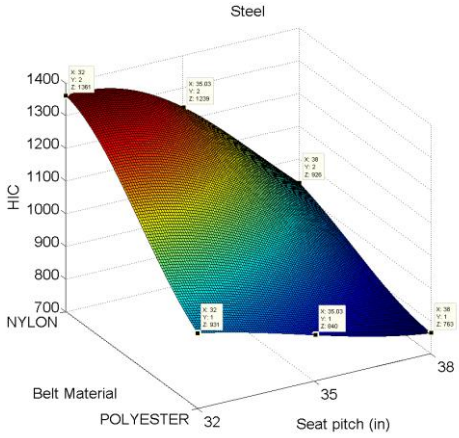

Figure 5.11: Surface plot of HIC for steel bulkhead for Part 25

Figures 5.12 and 5.13 are the surface plots of the head impact angle and head impact velocity for Part 25. From the plots we can observe that the head impact angle increases with the increase in seat pitch distances, for the belt materials of nylon and polyester. Similarly, for the head impact velocity, we can observe that the impact velocity is least for the seat pitch distance 38-in and highest for the seat pitch distance 35-in.

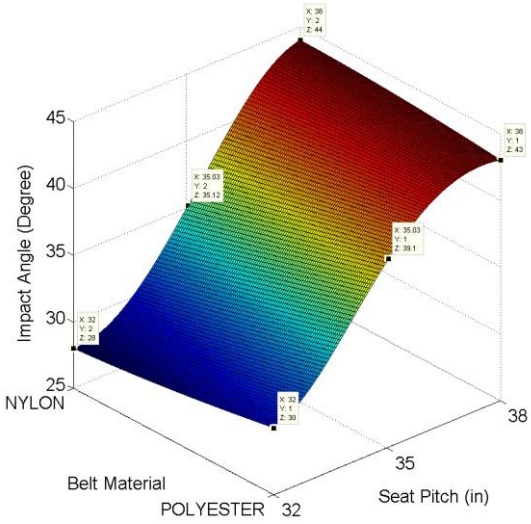

Figure 5.12: Surface plot of head impact angle for Part 25

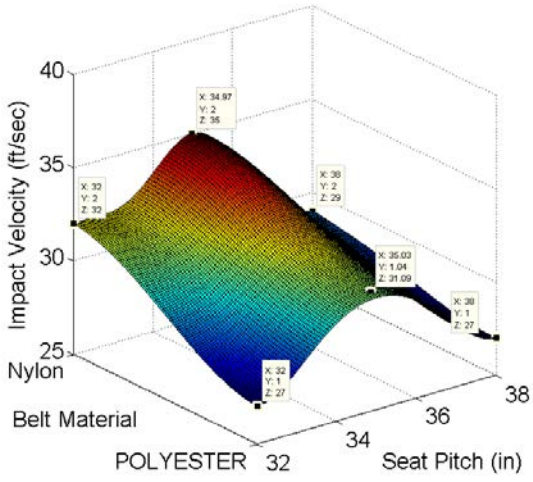

Figure 5.13: Surface plot of head impact Velocity Part 25

5.4.4 Combined Surface Plots for Aircraft Head Impacts

Figures 5.14 and 5.15 are the combined surface plots of the HIC for Part 23 Pilot, Passenger and Part 25, using the aluminum and steel bulkheads. The combined plots show the variations of HIC with different impact velocity and impact angle, with largest HIC values observed for the impact velocity of 50 ft/sec and the smallest HIC value observed for the impact velocity 27 ft/sec, for both aluminum and steel bulkheads.

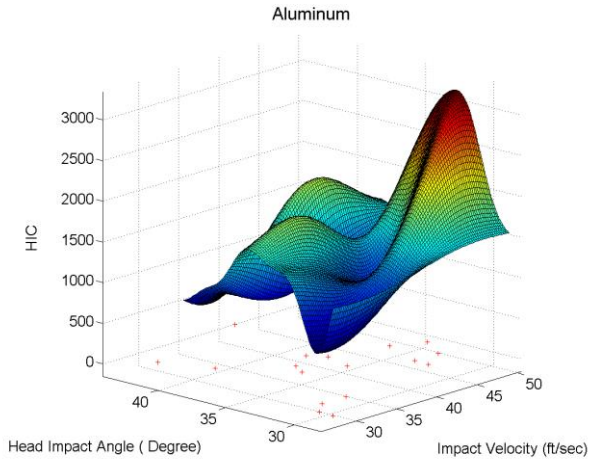

Figure 5.14: Combined surface plot of HIC from all data points for aluminum bulkhead

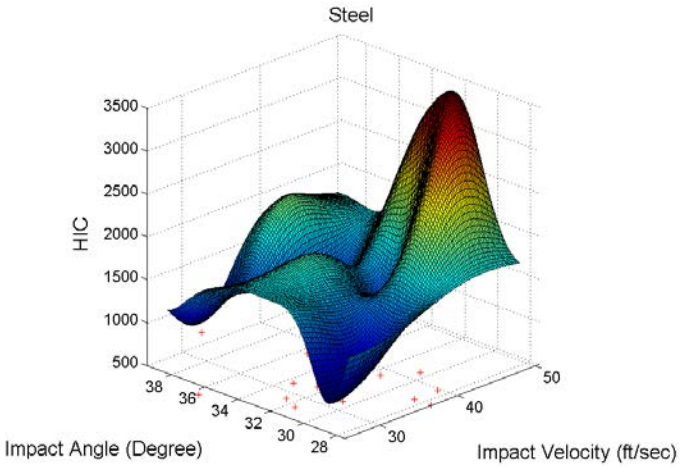

Figure 5.15: Combined surface plot of HIC from all data points for steel bulkhead

5.4.5 Cross Surface Plot for Aircraft Head Impacts

Figure 5.16 is the cross plot for the aircraft Part 23 Pilot, Passenger and Part 25 condition. The cross plot shows the variation of the HIC with the impact velocity and the bulkhead material of aluminum and steel material. From the plot we can observe that the HIC value increases with increase in impact velocity ft/sec, for both aluminum and steel bulkheads.

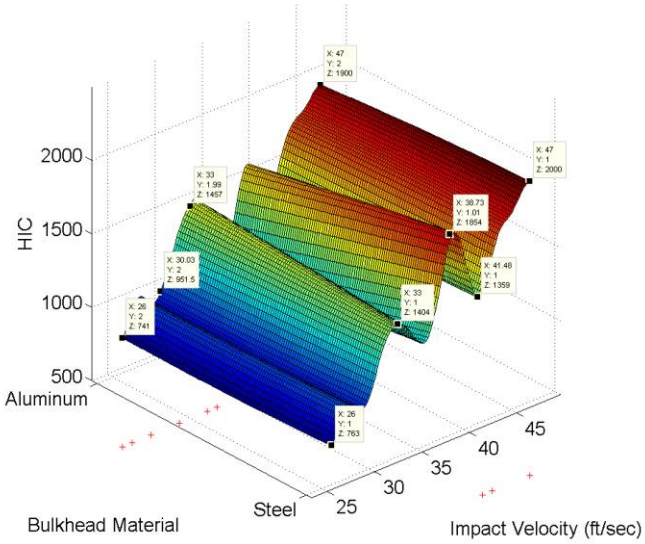

Figure 5.16: Cross plot for Aircraft Head Impact

Overall, figures through 5.2 to 5.16 represent the surface plots for the aircraft head impact conditions corresponding to the Part 23 Pilot and Passenger, and Part 25. The data points used in these surface plots are obtained from the Tables 4.1, 4.2 and 4.3 results. The response surfaces obtained for the HIC, impact angle and impact velocity, for both aluminum and steel bulkheads among all the three crash scenarios clearly indicates that the HIC values obtained for the FAR Part 25 is less than the permissible limit of 1000. Among the seat pitch distances, the lowest HIC was measured corresponding to the maximum seat pitch distance 38-in. We can also observe that the polyester belt material has better HIC protection compared to the use of nylon belt material.

5.4.6 Verification of Aircraft Surface Plots

The objective of this part of the section is to perform the response surface prediction by the Kriging method and selecting the sample data points from the surface plot. The sample points which are selected are the other data points from the surface plots, constructed by the given data points. This procedure is followed for all the surface plots obtained for the aircraft conditions. To achieve these objective, a set of four data points is selected from each surface plot, and these data points are used as input variables in the MADYMO computer simulations. The data points selected are compared with the results obtained from the actual simulations. The four new data points selected from each surface plots are speicifically: 33" seat pitch nylon belt, 33" seat pitch polyester belt, 36" seat pitch nylon belt, and 36" seat pitch polyester belt. Tables 4.2 shows the complete matrix of results obtained for the aircraft Part 23 pilot and passenger for the selected data points and the actual MADYMO computer simulation results and corresponding deviations.

Table 4.2: Validation of aircraft Part 23 pilot results for the selected data points

FAR PART 23 PILOT													
Seat Pitch (in)	Belt Type	Velocity (ft/sec)			Impact Angle (degree)			HIC (Steel)			HIC (Aluminum)		
		Result from Sample Points	MADYMO Result	% Error	Result from Sample Points	MADYMO Result	% Error	Result from Sample Points	MADYMO Result	% Error	Result from Sample Points	MADYMO result	% Error
33	Nylon	43	47	9%	32	32	0%	3237	3241	0.12%	2984	3027	1%
	polyester	43	44	2%	33	33	0%	2582	2596	0.53%	2327	2361	1%
36	nylon	43	48	12%	35	35	0%	2550	2490	3%	2298	2201	4%
	polyester	43	45	5%	36	36	0%	1539	1527	0.77%	1311	1379	5%

Tables 4.3 and 4.4 show the complete matrix of results obtained for the aircraft Part 23 pilot and passenger conditions for the selected data points and the actual MADYMO simulation results.

Table 4.3: Validation of aircraft Part 23 passenger results for the selected data points

FAR PART 23 PASSENGER													
Seat pitch	Belt Type	Velocity (ft/sec)			Impact Angle (degree)			HIC (Steel)			HIC (Aluminum)		
		Result from Sample Points	MADYMO Result	% Error	Result from Sample Points	MADYMO Result	% Error	Result from Sample Points	MADYMO Result	% Error	Result from Sample Points	MADYMO result	% Error
33	Nylon	44	45	2%	33	33	0%	2042	2067	1%	1962	1947	0.76%
	polyester	40	42	5%	34	34	0%	1480	1407	5%	1434	1491	4%
36	nylon	46	47	2%	40	41	2%	1586	1607	1%	1561	1552	1%
	polyester	40	40	0%	38	40	5%	1098	1090	0.72%	1031	1063	3%

Table 4.4: Validation of aircraft Part 25 results for the selected data points

FAR PART 25													
Seat Pitch (in)	Belt Type	Velocity (ft/sec)			Impact Angle (degree)			HIC (Steel)			HIC (Aluminum)		
		Result from Sample Points	MADYMO Result	% Error	Result from Sample Points	MADYMO Result	% Error	Result from Sample Points	MADYMO Result	% Error	Result from Sample Points	MADYMO result	% Error
33	Nylon	32	32	0%	29	30	3%	1354	1371	1%	1335	1331	1 %
	polyester	28	29	4%	32	32	0%	904	924	1%	888	874	1 %
36	nylon	33	33	0%	39	40	3%	1145	1099	4%	1140	1137	0.26%
	polyester	30	30	0%	42	42	0%	809	821	1%	792	721	9%

From Tables 4.2, 4.3 and 4.4, one can observe the percentage deviation (error) in the selected sample points and the MADYMO simulation results is quite minimal, with 2-6% difference between the actual model and predicted data for the impact angle, impact velocity, and approximately a difference of 10-12% for the HIC. This hence demonstrates that the Kriging model reasonably predicts the response of the system.

Figure 5.17 shows sample plots for impact velocity to show the comparission of surface plot between the 6 data points and 10 data points. As observed, the plot with more data points have a better and smoother response surface when compaired to the one plot with 6 data points.

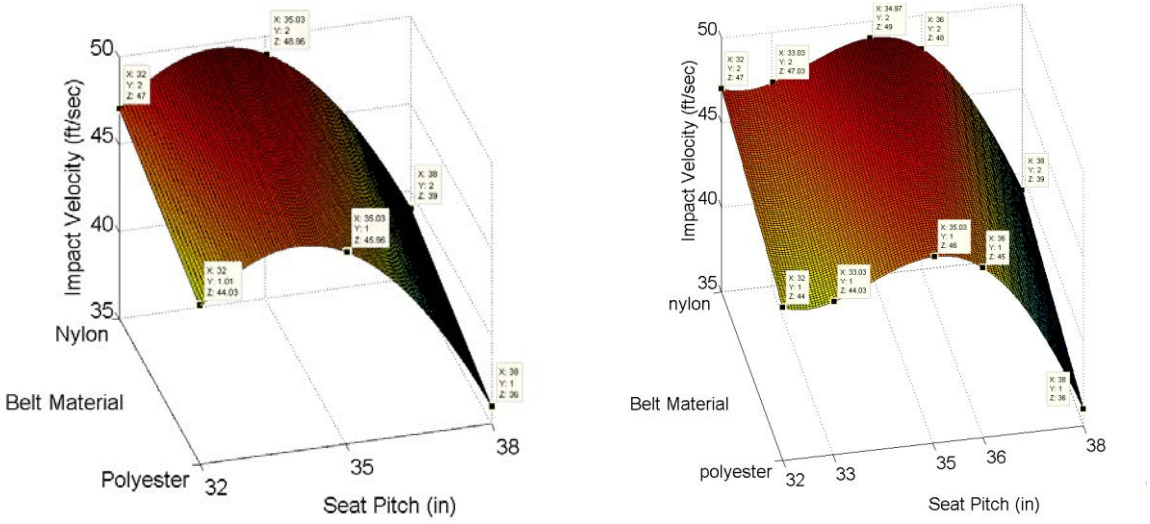

(a) (b)

Figure 5.17: Comparison of surface plot for different number of sample points with (a) representing 6 data points and (b) representing 10 data points.

5.5 Surface Plots for Automotive Head Impact

Figures 5.18 and 5.19 are the surface plots of the HIC for the aluminum and steel impact surface for automotive conditions. From the plots we can observe that the HIC value decreases with the increase in the distance between the steering representation and dummy head, as the 3-point belt contrains the occupant significantly impacting onto the steering surface. We can also observe that the HIC values obtained for the polyester belt are slightly lower when compared to the nylon belt material.

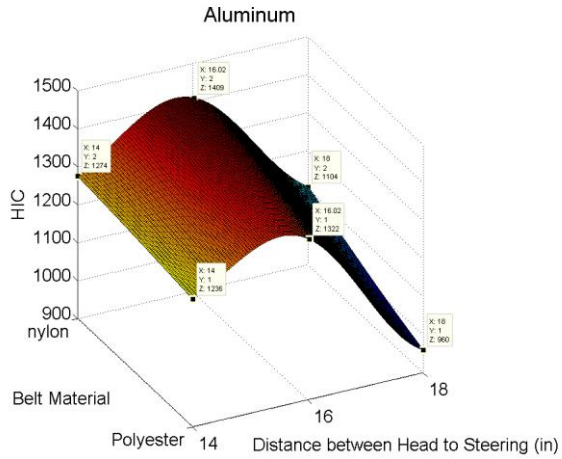

Figure 5.18: Surface plot of HIC for automotive of impact surface aluminum material

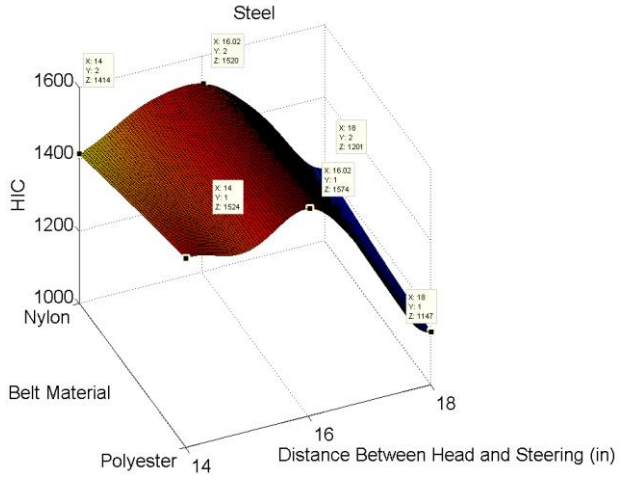

Figure 5.19: Surface plot of HIC for automotive of impact surface Steel material

Figures 5.20 and 5.21 are the surface plots of the head impact angle and head impact velocity for the aluminum and steel material steering representation for automotive condition. From the plots we can observe that the head impact angle increases with the increase in the distance between the steering representation and dummy head, for the nylon and polyester belt materials. Similarly, for the head impact velocity, we can observe that the impact velocity is least for the distance 18-in and highest for the distance 15-in between head and steering.

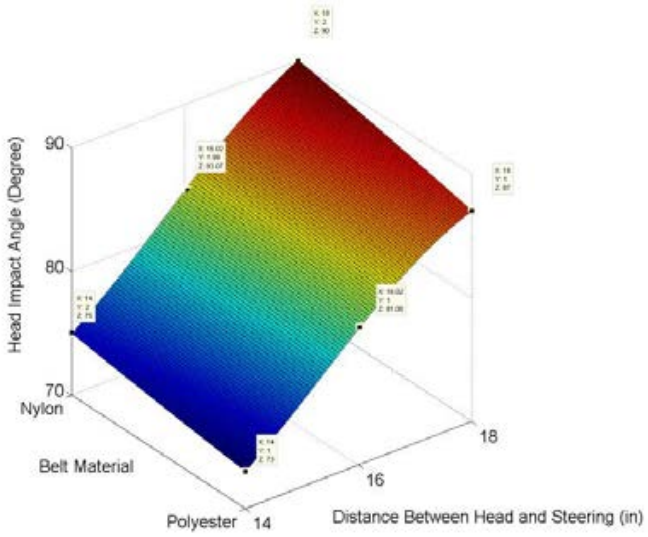

Figure 5.20: Surface plot of impact angle for automotive condition

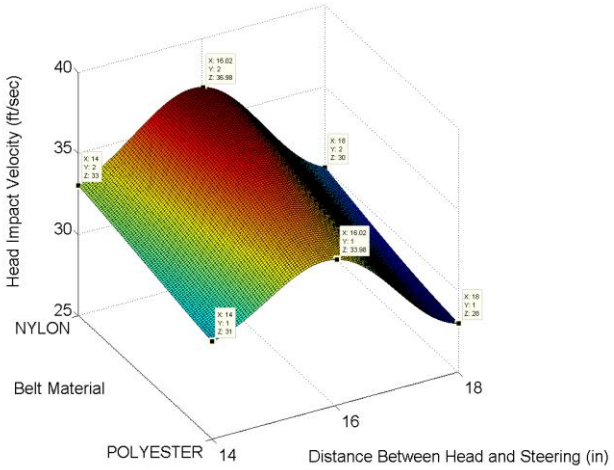

Figure 5.21: Surface plot of impact velocity for automotive condition

5.6.1 Combined Surface Plots for Automotive Head Impacts

Figures 5.22 and 5.23 are the combined surface plots of the HIC for the aluminum and steel steering representations for automotive condition. The plots illustrate all the results obtained for the automotive are in one single plot. From the combined plots, we can observe that the HIC value tends to increase with an increase in head impact velocity. Where as, the impact angle does not follow any significant pattern for the variation in HIC.

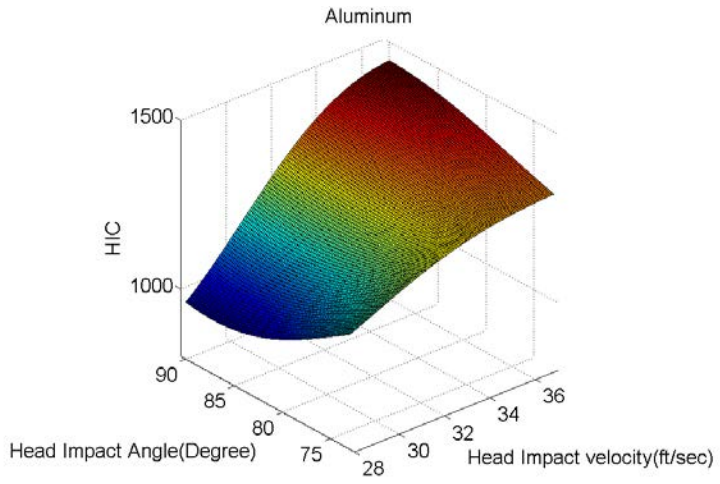

Figure 5.22: Combined surface plot of the HIC from all data points on impact on aluminum material

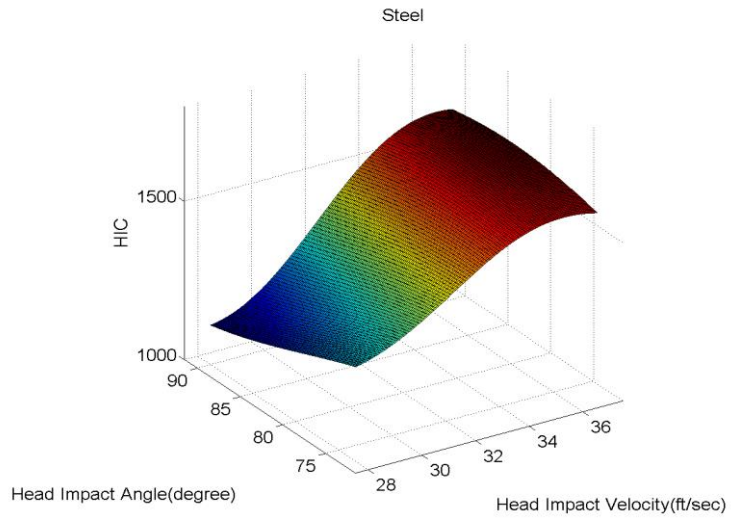

Figure 5.23: Combined surface plot of the HIC from all data points on impact on steel material

5.6.2 Cross Surface Plot for Automotive Head Impacts

Figure 5.24 is a cross plot for the automotive impact. From the cross plot, we can observe that the HIC value increases with the increase in impact velocity of the head when impacted on the steering representation for both aluminum and steel materials.

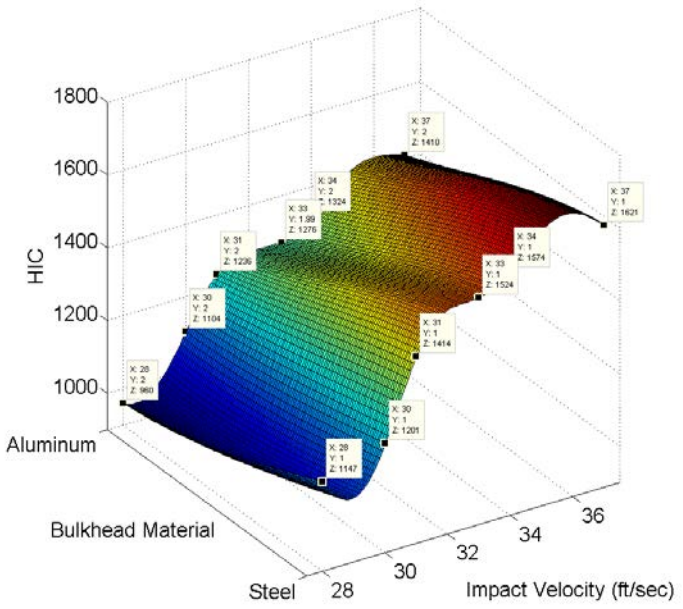

Figure 5.24 : Cross plot for automotive

Overall, figures through 5.18 to 5.24 represent the various surface plots for the automotive head impact cases. The data points used in these surface plots are obtained from the Table 4.4 results. The response surface obtained for the HIC generally shown smaller HIC for the automotive cases when compared to aircraft cases. Among the distances between impact surface and dummy head, the lowest measured HIC was corresponding to the maximum the distance of 18-in, as the motion is restrained by using the 3-point belt. We can also observe that the polester belt material polyester provides a better HIC protection when compared to the nylon belt material.

5.6.3 Verification of Automotive Surface Plots for Head Impact

The verification of the surface plot for automotive is conducted to study the response surface prediction by the Kriging method by selecting the sample data points from the surface plot. To achieve this objective, a set of two data points is selected from each surface plot for automotive case, and these data points are used as input variables in the MADYMO computer simulation. The two new data points selected from each surface plot for specifically:17" distance between the dummy head and steering representation and nylon belt, 17" distance between the dummy head and steering representation polyester belt.

The results obtained for the validation of response surface data validation for the selected data points and the actual MADYMO computer simulation results for the automotive are shown in Table 4.5.

Table 4.5: Validation of automotive results for the selected data points

	Belt Type	Velocity (ft/sec)			Impact Angle (degree)			HIC (Steel)			HIC (Aluminum)		
Distance Between dummy head and steering representation (in)		Result from Sample Points	MADYMO Result	% Error	Result from Sample Points	MADYMO Result	% Error	Result from Sample Points	MADYMO Result	% Error	Result from Sample Points	MADYMO result	% Error
17	Nylon	33	34	3%	87	88	1 %	1414	1360	4%	1268	1230	3%
	Polyester	31	33	6%	85	87	2%	1414	1304	8%	1268	1098	13%

From Table 4.5, we can observe that the results obtained for the automotive case for the sample points are selected on the surface plots are quite close to the ones from actual MADYMO

simulations. The percentage difference is quite minimal, proving that the Kriging method reasonably predicts the response of the system. The Kriging model response surface data were found to be with 1-6 % difference between actual model model and predicted data for the impact angle, impact velocity, and approximately a difference of 3-13% for the HIC.

Figure 5.21 show a sample surface plots for the head impact angle comparisson of surface plots between the 6 data points and 10 data points. From the figure, we can observe that the plot with more data points has a better and smooth response surface when compared to the plot with 6 data points.

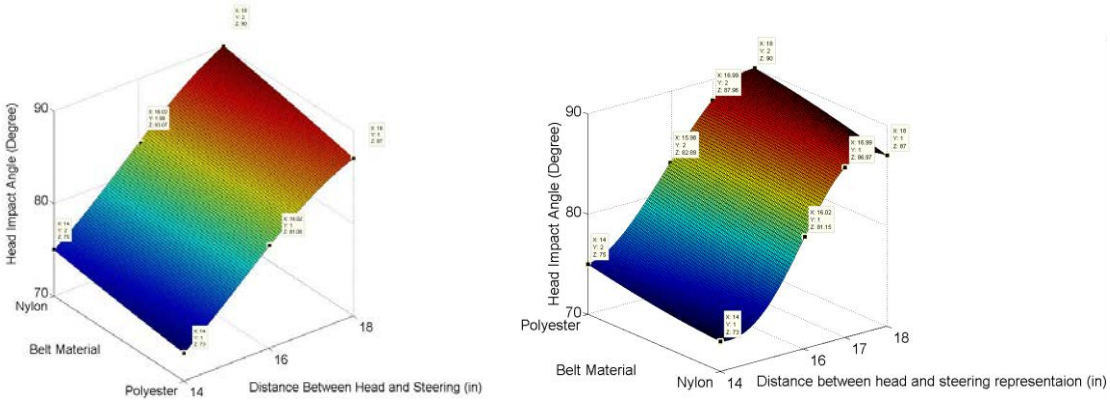

(a) (b)

Figure 5.25: Comparison of automotive surface plots for different number of sample points with (a) representing 6 data points, and (b) representing 10 data points

CHAPTER 6

CONCLUSIONS AND RECOMMENDATIONS

6.1 Conclusions

The objective of this research was to develop a set of response surface data for the evaluation of HIC with the consideration of different parameters in various automotive and aircraft impact scenarios. Using aircraft seat certification standards, defined by FAR Part 23 Pilot, Passenger and Part 25, MADYMO computer models were developed and simulations were run for 54 different input conditions, using different parameters such as seat pitch, bulkhead stiffness, and belt properties.

Using the FMVSS regulation, an FE model of a typical sedan in frontal impact was utilized and simulated. The acceleration pulse was then applied to the MADYMO occupant model. A total of 24 simulation runs were performed for different input conditions, using different parameters such as belt properties, stiffness of impact surface material, and distance between the dummy head and impact surface.

From the stimulations obtained from all the categories of aircraft (both pilot and passenger), it is observed that the impact angle increases with an increase in seat pitch from 32-in to 38-in for about 20%, and the impact velocity remains nearly the same, but the HIC is reduced about 10%. The lowest HIC corresponds to a maximum seat pitch distance of 38 in, for which the head only glances through the impact surface.

From the simulations obtained for the automotive case, it was observed that with an increase in the distance from the head and impact surface, the HIC is reduced. The minimum HIC is obtained for the distance from the head to the steering representation of 18-in, as the motion of the torso is restrained by the three-point belt.

The results obtained corresponding to the use of the polyester belt show better HIC protection compared to the nylon belt. For the Part 25 conditions, the HIC values were below the 1000 for all seat pitch distances, when the polyester belt is used. The nylon belt produces larger extension and has less energy absorption capability during a crash. Due to this, the HIC values obtained for the nylon belt cases exceed in the permissible value in almost all of the simulations.

The HIC values, overall are found to be increasing with increase in stiffness (aluminum to steel) of the impact surface for about 15%, in both automotive and aircraft impact test cases. In almost all scenarios, the HIC obtained is considered to be above the permissible limit of 1000 (with 36-ms maximm window size) for both materials of impacting the surface. The exception was for the Part 25 and Part 23 passenger cases for the larger seat pitch distance. It must be noted though that all the HIC results obtained in this thesis correspond to the use of a rigid seat where no energy is absorbed, and hence the HIC results demonstrate worst-case scenarios.

The HIC value are found to be increasing with an increase in the head velocity in both aircraft and automotive impact cases. With an increase of 30% in head impact velocity, the HIC values increase by 50%. Whereas, the HIC values are found to be decreasing with an increase in the head impact angle, but not significantly. With 20 % increase in head impact angle, there is a decrease of 14% in the resulting HIC.

The Kriging method reasonably predicts the response of the system with the consideration of all parameters. The Kriging model response surface data are found to be with 2-6% difference between the actual model from MADYMO simulation and predicted data from the surface plots for impact angle, impact velocity, and approximately a difference of 10-12% for the HIC value.

Overall, the collective results of many simulations of this thesis as the surface plots generated could be of significant use to the designers of automotive seats and aircraft interiors and in coming up with the most promising designs for occupant head impact protection in various frontal crash scenarios.

6.2 Recommendations

Based on many simulations cases, conclusions made and results obtained from the study, the following are the recommendations for further study on the topic.

- For the head impact surface, a softer material or different stiffness can be considered and the corresponding HIC data can be generated.
- The results are obtained for the current FAR regulations for aircraft impact conditions. Other conditions and impact crash scenarios can also be investigated.
- For the automotive condition, a simple frontal impact barrier was simulated. One might examine the newer regulations such as the small overlap, oblique impact, etc. Further, many other real world accident scenarios can also be investigated and the data on the impact angle, impact velocity, and the HIC results can be expanded.
- This study is restricted to the front-row passengers coming into direct contact with the aircraft bulkhead or the car steering representation. The passengers in the rear seats may also subjected to head injuries in a aircraft bulkhead "row-to-row", or the automotive back seat crash scenarios and simulations can be carried out to obtain the HIC changes.
- Further safety features could be added to the FE model and simulation, such as air bags, padding material on the impact surface, and the HIC responses can be examined.
- The effect of energy-absorption of seats could also be added to the study by development and simulation of FE model of the seat.

REFERENCES

REFERENCES

[1] Traffic Safety Facts, "Motor Vehicle Crash Data National Highway Traffic Safety Administartion," [Cited April, 2016].

[2] Aviation safety network, https://aviation-safety.net/statistics/, [Cited April, 2016].

[3] FAA Regulation, WWW.faa.gov, [Cited April, 2016].

[4] Federal Motor Vehicle Safety Standards and Regulation, http://www.nhtsa.gov/cars/rules/import/fmvss/, [Cited April, 2016].

[5] Lankarani, H. M., and Nikravesh, P. E., "A Contact Force Model With Hysteresis Damping For Impact Analysis Of Multibody Systems," *Journal of Mechanical Design*, 112, 1990.

[6] Lankarani, H. M., and Nikravesh, P. E., "Continuous Contact Force Model for Impact Analysis in Multibody Analysis in Multibody Systems," *Nonlinear Dynamics* 5 (2), 193-207, 1994.

[7] Lankarani, H. M., and Nikravesh, P. E., "Hertz Contact Force Model with Permanent Indentation in Impact Analysis of Solids," ASME Design Engineering Division DE 44, 391-395, 1992.

[8] Flores, P., and Lankarani, H. M., **Contact Force Models for Multibody Dynamics**, Springer 2016.

[9] Hutchinson, J., Kaser, M.J., and Lankarani, H. M., "The Head Injury Criterion (HIC) Functional," *Applied Mathematics and Computation* 96 (1), 1-16, 1998.

[10] Lankarani, H. M., Malapati, S. R., and Menon, R., "*Evaluation of Head Injury Criteria*," WSU/NIAR, 1993.

[11] Zhang, Z., Xu, L., Flores, P., and Lankarani, H. M., "A Kringing Model for Dynamic of Mechanical Systems with Revolute Joint Clearances,"*Journal of Computational and Nonlinear Dynamics*, 9031013-13p, 2014.

[12] Zhang, Z., "A Design of Experiment and Kriging-Based Model for Study the Dynamic of Multibody Mechnaical System with Revolute Joint Clearance," MS Thesis, Wichita State University, 2013.

[13] Lankarani, H. M., Ma, D., and Menon, R., "Impact Dynamic of Multibody Mechanical System and Apllication to Crash Response of Aircraft Occupant/Structure," in Computational Dynamics in Multibody Systems, 239-265, 1995.

[14] Lankarani, H. M., "*Current Issue Regarding Aircraft Crash Injury Protection*," Crashworthiness of Tranportation Systems: Structural Imapct and Occupant, 1997.

[15] Lankarani, H. M., Ma, D., and Menon, R., "Occupant Dynamic Responses for Evaluation of Compliance Charcteristics of Aircraft Bulkheads," 18th Annual ASME Design Automation Conference, 377-382, 1992.

[16] Deweese, R., Moorcraoft, D., Thorbole, C. K., and Lankarani, H. M., "Use of Head Component Tester to Evaluate the Injury Potential of an Aircraft Head –up Display," *International Journal of Crashworthiness,* 16(4), 385-395, 2011.

[17] Thorbole, C. K., and Lankarani, H. M., "Performance Evaluation of HIC Component Testing Device With a Flexible Neck Using Computational Model," ASME 2008 International Engineering Congress and Exposition, 423-429, 2008.

[18] Nagarajan, H., McCoy, M., and Lankarani, H. M., "Design of HIC Complicant Aircarft Bulkheads and Cabin Class Divider Panels," *International Journal of Crahworthiness*, 10(5) 525-534, 2005.

[19] Lankarani, H. M., Olivares, G., and Nagarajan, H., "A virtual Multibody and Finite Element Analysis Environment in the Field of Aerospace Crashworthiness," in Virtual Nonlinear Multibody Systems, 187-212, 2003.

[20] Ma, D., Menon, R., and Lankarani, H. M., "Impact Dynamics of Multibody Mechanical Systems and Application to Crash Response of Aircraft Occupant/Structure,''in NATO-Advanced Study Institute on Computer Aided Analysis of Rigid and Multibody System," 1993.

[21] Lankarani, H. M., Ma, D., and Ermer, G., "Biodynamic Simulations of an Aircraft Pilot/Passenger in Various Crash Environments," 1990.

[22] Lankarani, H. M., Koshy, C.S., and Thorbole, C.K., ''Design and Validation of a Component Head Injury Criteria Tester for Aerospace Application,'' ASME 2005 International Design Engineering Technical Conferences, 2005.

[23] Ma, D., and Lankarani, H. M., "Computer Simulations of an Occupant-Restarint System," Proceedings: Teckfest 17 p 20 (See N 91-18004 10-01) 1991.

[24] Thorbole, C.K., and Lankarani, H. M., "Performance Evaluation of Component HIC Component Tester for Aerospace Applications," SAE Technical Paper, 2008.

[25] Nagarajan, H., McCoy, M., Koshy, C.S., and Lankarani, H. M., "Design, Fabrication and Testing of a Component HIC Tester for Aircraft Applications," *International Journal of Crashworthiness*, 10(5), 515-523, 2005.

[26] Hooper, S. J., Lankarani, H. M., and Mirza, M. C., "Parametric Study of Crashworthy Bulkhead Designs," FAA Report, March 2001.

[27] Hooper, S. J., and Lankarani, H. M., "Application of Computer-Aided Analysis Tools for Aircraft Occupants and Seat Crashworthiness Problems," *International Journal of Crashworthiness*, 4(4), 443-448, 1999.

[28] Lankarani, H. M., Hooper, S. J., Mirza, M. C., and Sivakumaran, S., "Attenuation and Simplified Testing Procedure of HIC for Aircraft Crash,'' SAE Technical Paper, 1997.

[29] Lankarani, H. M., "Contact/Impact Dynamics Applied to Crash Analysis," Crashworthiness of Transportation Systems: Structural Impact and Occupant, 1997.

[30] Lankarani, H. M., and Aravinthan, S., "Design of Non-Sled Setup to Measure Head Injury Criteria,"WSU/NIAR, 1993.

[31] Thorbole, C.K., and Lankarani, H. M., "Performance Evaluation of Computation HIC Component Testing Device With a Flexible Neck Using Computational Model," ASME International Mechanical Engineering Congress and Exposition, 423-429, 2008.

[32] Lankarani, H. M., "Injury Bio-Mechanics Lecture," Wichita State University, 2016.

[33] Steele, B., and Lankarani, H. M., "A Brief Examination and Comparison between the Federal Aviation Regulations," National Institute for Aviation Research Tech. Rep, 1991.

[34] Moradi, R., Thorbole, C.K., McCoy, M., and Lankarani, H. M., "Biodynamic Modelling of a Pedestrian Impact of a Pedestarin Impact With a Rigid Frontal Guard of a Utility Vehicle," *ASME 2010 International Mechanical Engineering Congress and Exposition*, 57-65, 2010.

[35] Lankarani, H. M., "Design and Valiation of NIAR Component HIC Tester for FAR Part 23/25 Aircraft Seat Certification," FAA CAMI, 2004.

[36] FE Car model Information, http://www.ncac.gwu.edu/vml/models.html, [Cited April, 2016].

[37] Prabhu, G., "Parametric study of Head Paths and HIC Data for Aircraft seat and Cabin Interior Certification," MS Thesis, Wichita State University, 2006.

[38] Sprague, M.AA and Geers T.S, "A Spectral-Element Method for Modeling Cavitaions in Transient Fluids- Struture Interaction," *International Journal for Numerical Methods in Engineering*, Vol. 60 No. 15, pp 2461-2499, 2004.

[39] MADYMO reference manual, version 7.5, TASS INETRNATIONAL, [cited April, 2016].

[40] LS DYNA Apllications, http:///www.lstc.com [Cited April, 2016].